**SUPPORTING INFORMATION**

# Transforming $PPh_3$ into Bidentate Phosphine Ligands at Ru-Zn Heterobimetallic Complexes

Niall O'Leary, Fedor M. Miloserdov, Mary F. Mahon and Michael K. Whittlesey

*Department of Chemistry, University of Bath, Claverton Down, Bath BA2 7AY, U.K.*

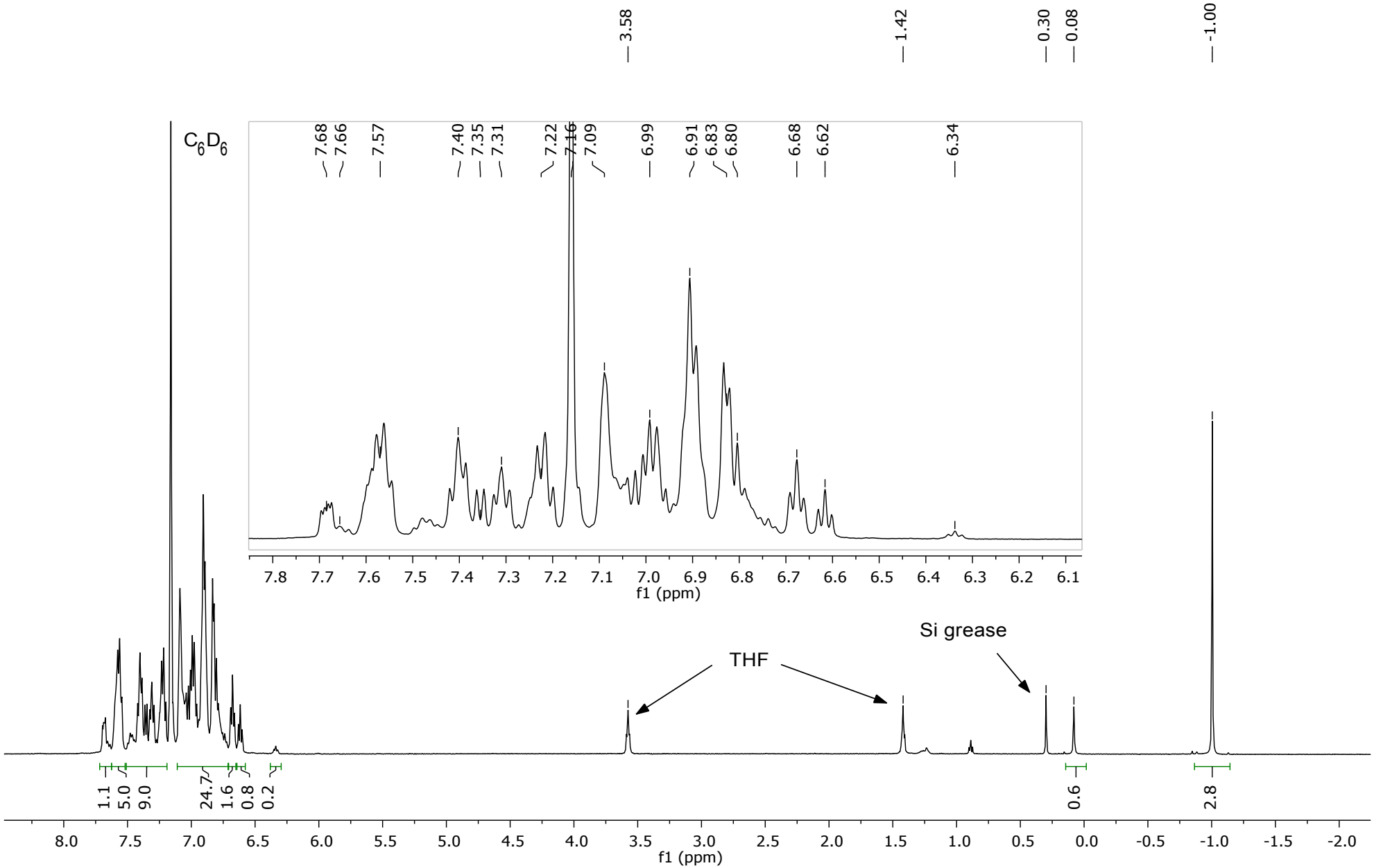


**Fig. S1.** $^{1}$H NMR spectrum (500 MHz, $C_6D_6$, 298 K) of [Ru(dppbz)($PPh_2$(biphenyl)′)ZnMe] (**1**).

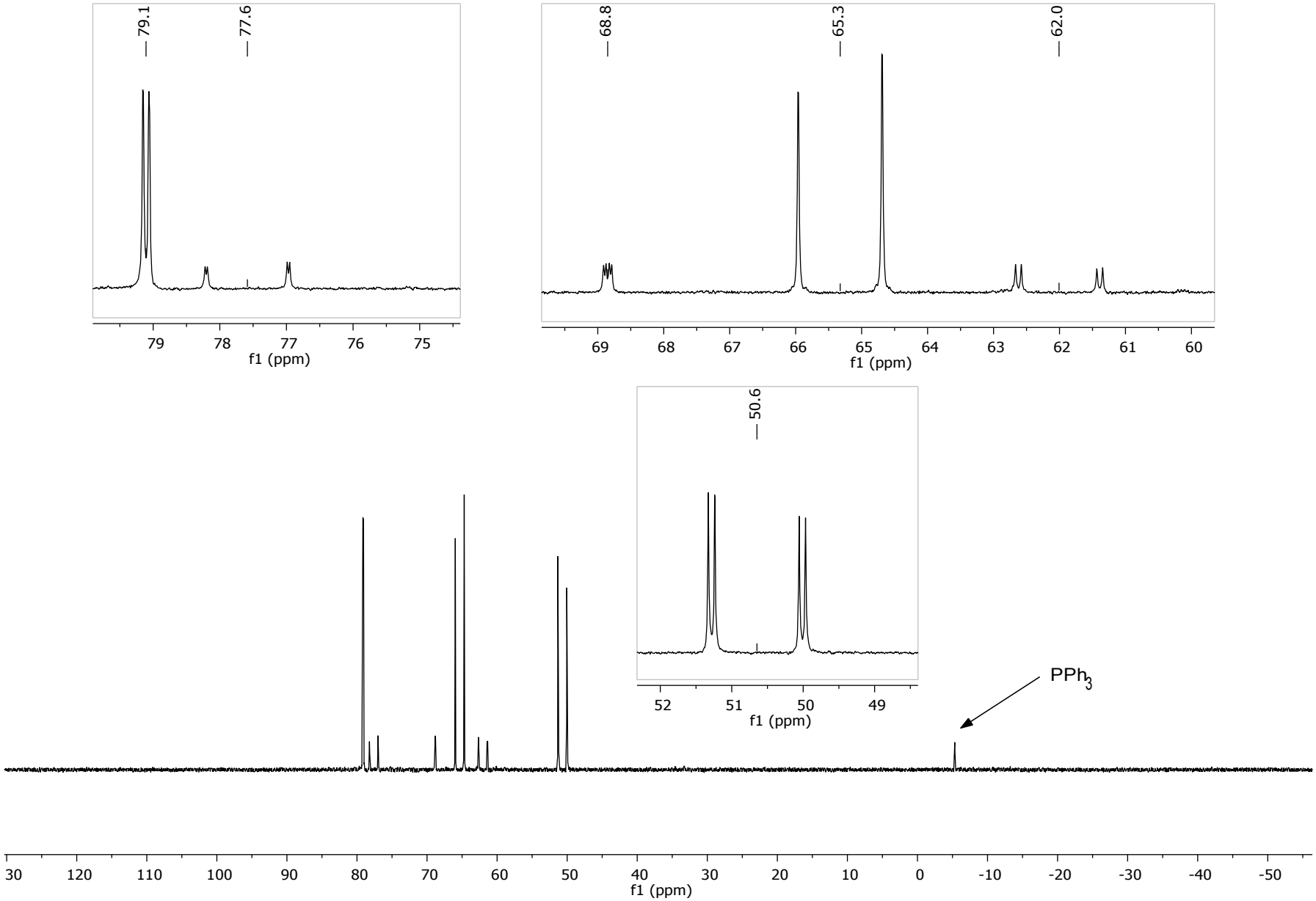


**Fig. S2.** $^{31}P\{^{1}H\}$ NMR spectrum (202 MHz, $C_6D_6$, 298 K) of [Ru(dppbz)($PPh_2$(biphenyl)′)ZnMe] (**1**).

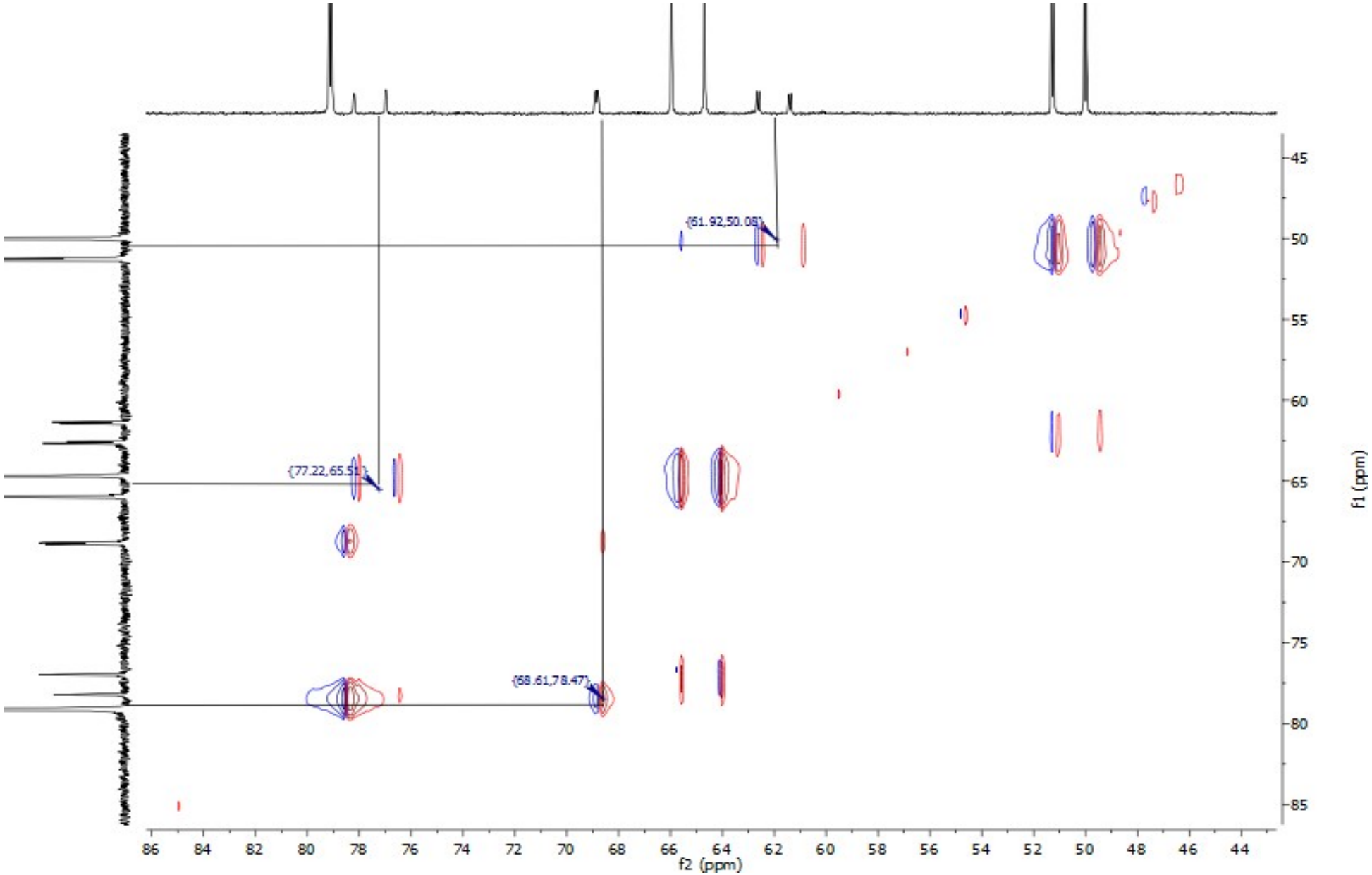


**Fig. S3.** $^{31}P\{^{1}H\}$ EXSY (202 MHz, $C_6D_6$, 298 K) of [Ru(dppbz)($PPh_2$(biphenyl)′)ZnMe] (**1**).

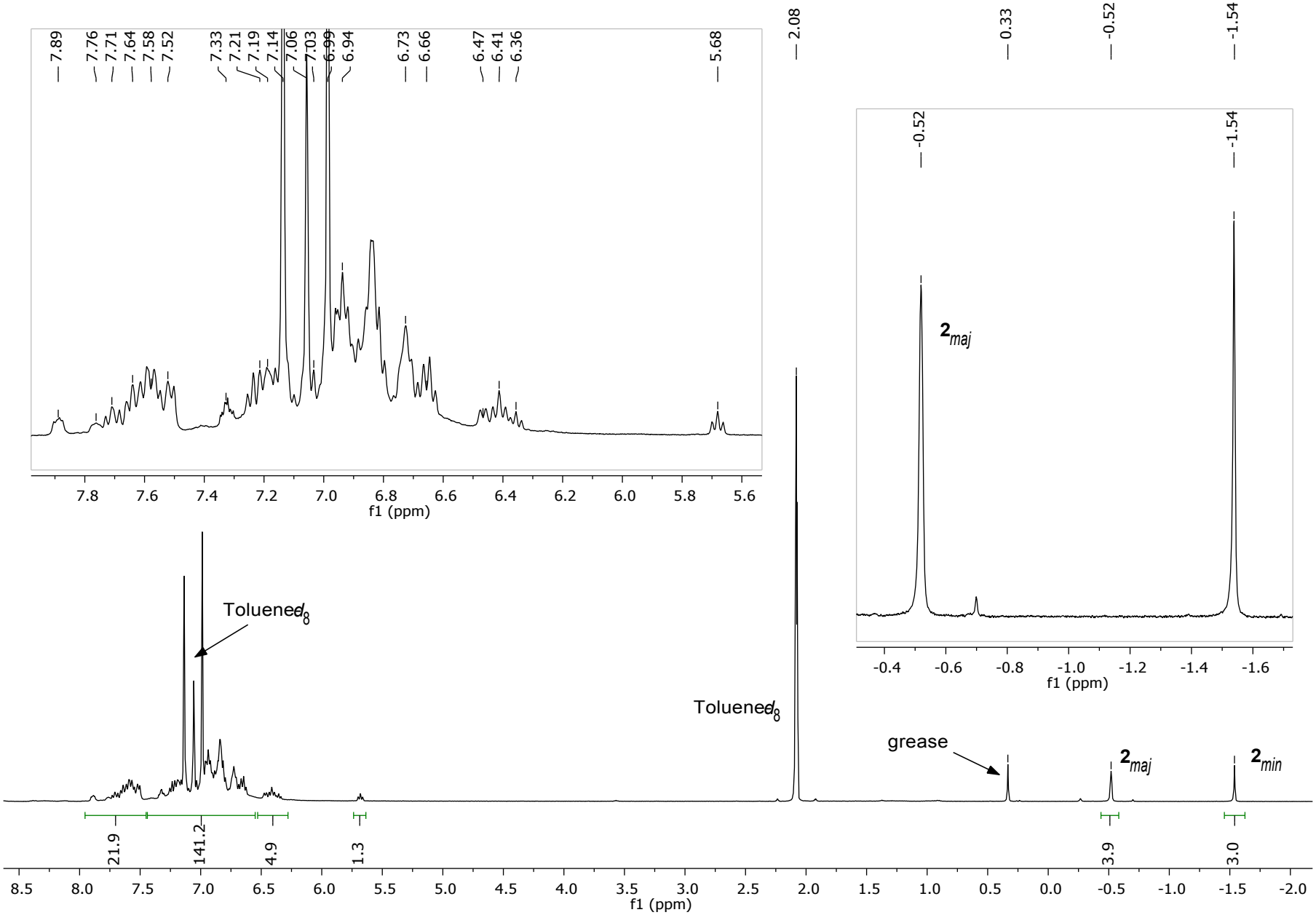


**Fig. S4.** $^{1}$H NMR spectrum (400 MHz, $C_6D_5CD_3$, 223 K) of [Ru(dppbz)($PPh_2$(biphenyl)′)(CO)ZnMe] (**2**), generated from **1** and CO.

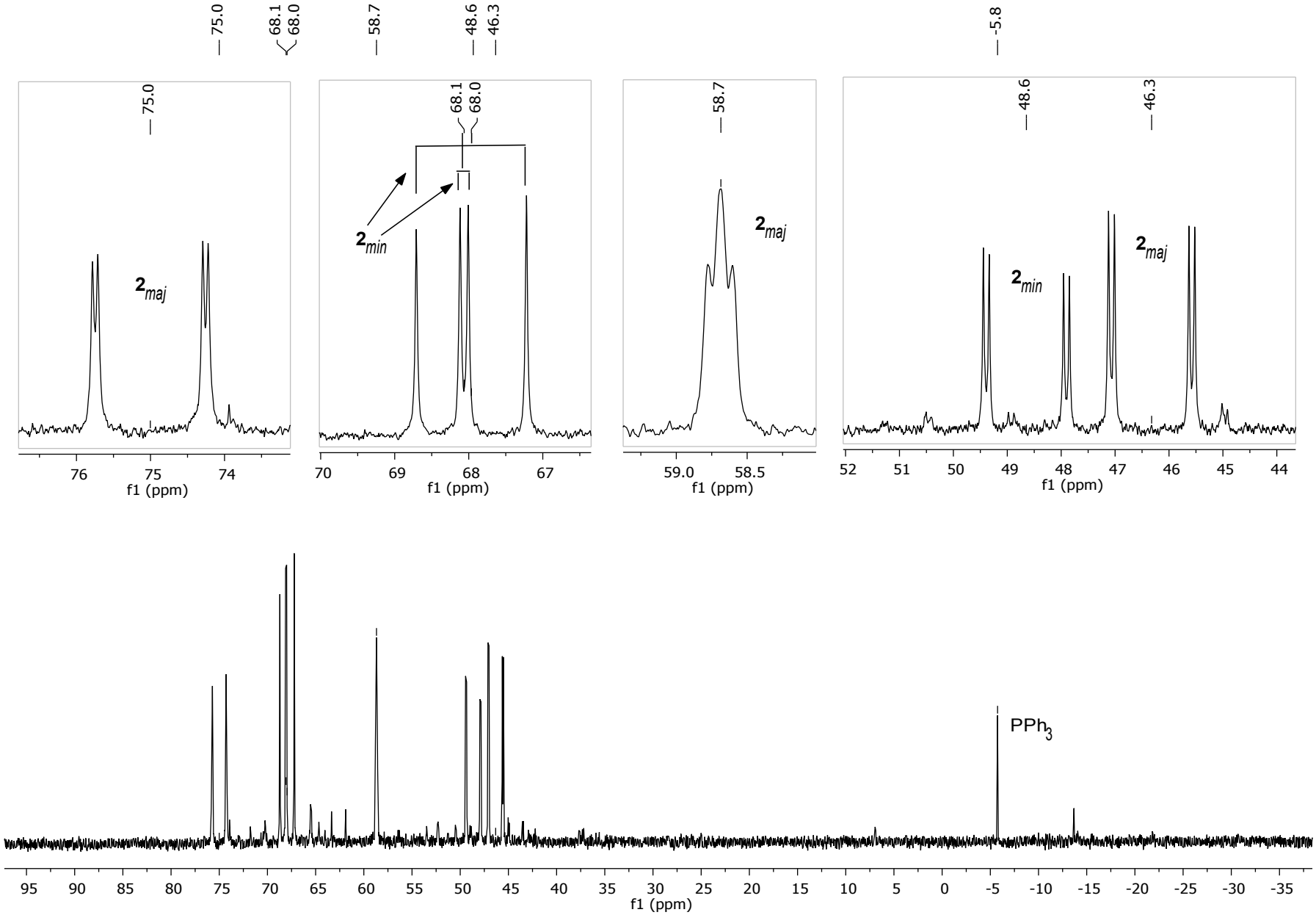


**Fig. S5.** $^{31}P\{^{1}H\}$ NMR spectrum (162 MHz, $C_6D_5CD_3$, 223 K) of [Ru(dppbz)($PPh_2$(biphenyl)′)(CO)ZnMe] (**2**), generated from **1** and CO.

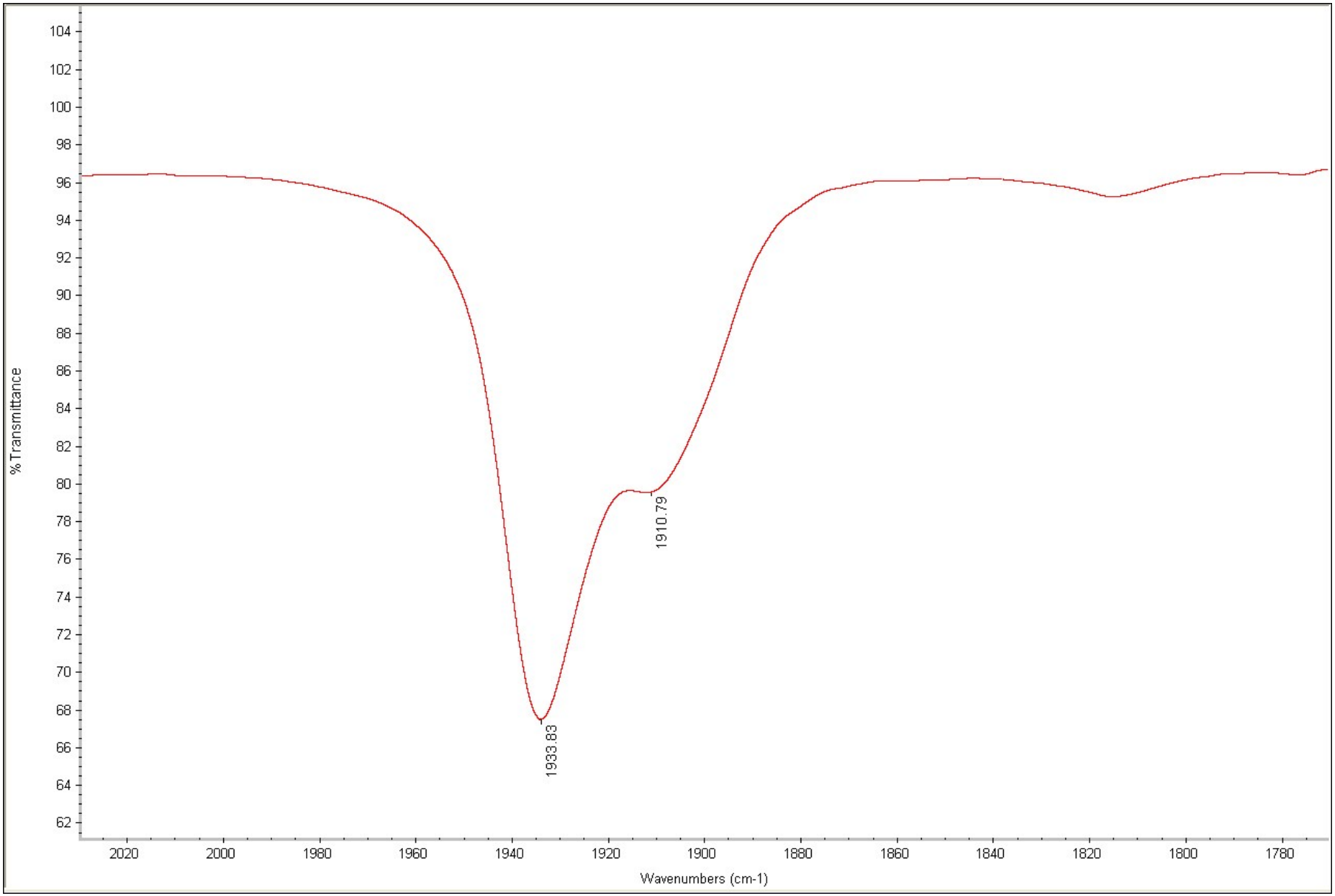


**Fig. S6.** IR spectrum (in $C_6D_5CD_3$) showing carbonyl bands for the two diastereomers of Ru(dppbz)($PPh_2$(biphenyl)′)(CO)ZnMe] (**2**).

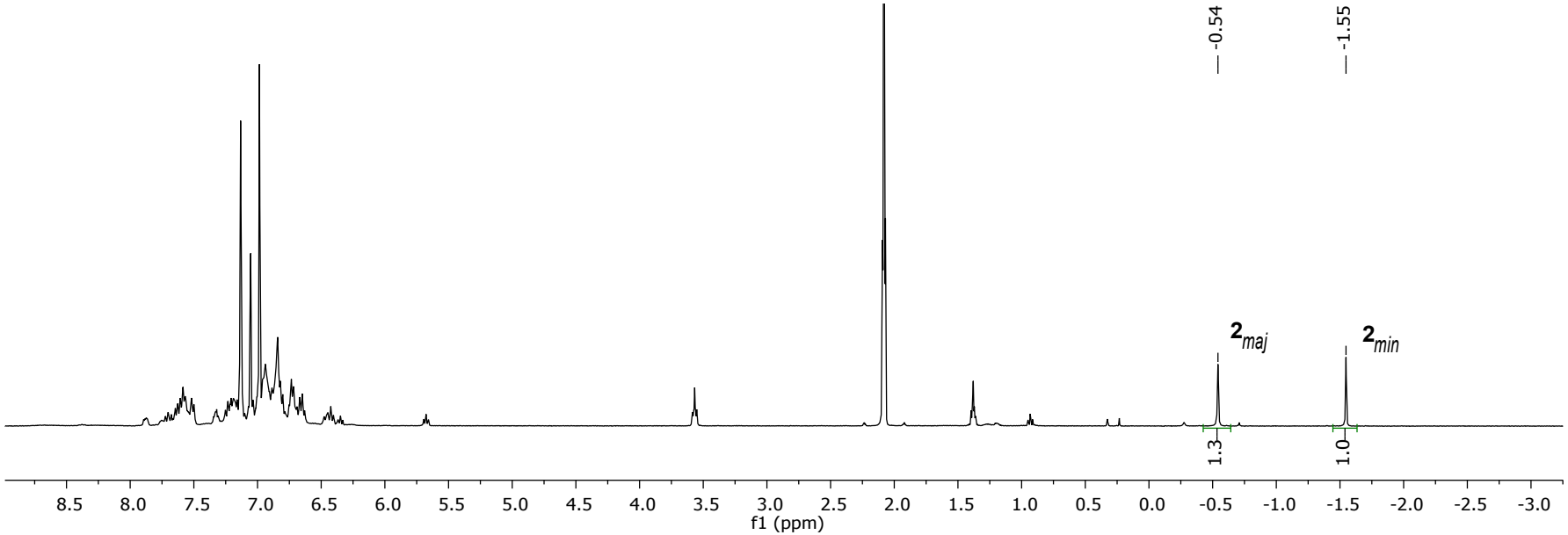


**Fig. S7.** $^{1}H$ NMR spectrum (400 MHz, $C_6D_5CD_3$, 223 K) of [Ru(dppbz)($PPh_2$(biphenyl)′)($^{13}CO$)ZnMe] (**2**), generated from **1** and $^{13}CO$.

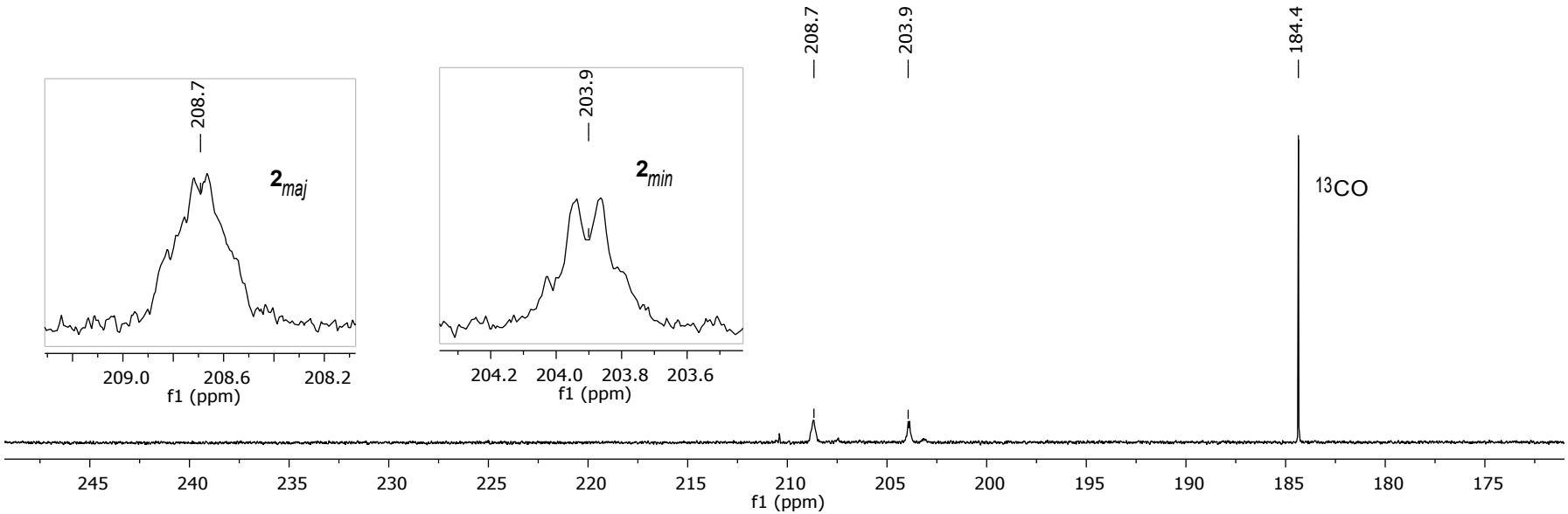


**Fig. S8.** $^{13}C\{^{1}H\}$ NMR spectrum (101 MHz, $C_6D_5CD_3$, 223 K) of [Ru(dppbz)($PPh_2$(biphenyl)′)($^{13}CO$)ZnMe] (**2**), generated from **1** and $^{13}CO$.

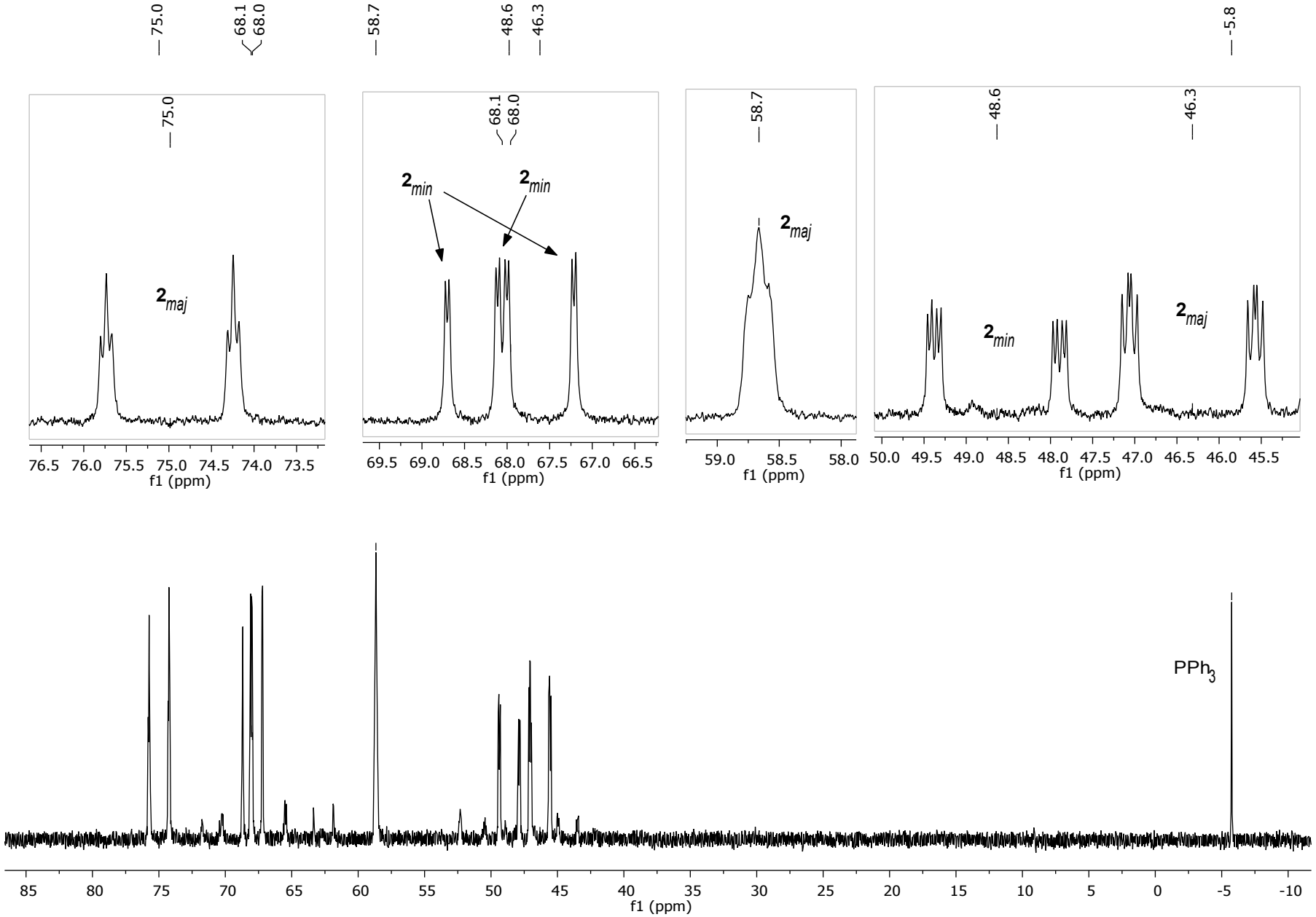


**Fig. S9.** $^{31}P\{^{1}H\}$ NMR spectrum (162 MHz, $C_6D_5CD_3$, 223 K) of [Ru(dppbz)($PPh_2$(biphenyl)′)($^{13}CO$)ZnMe] (**2**), generated from **1** and $^{13}CO$.

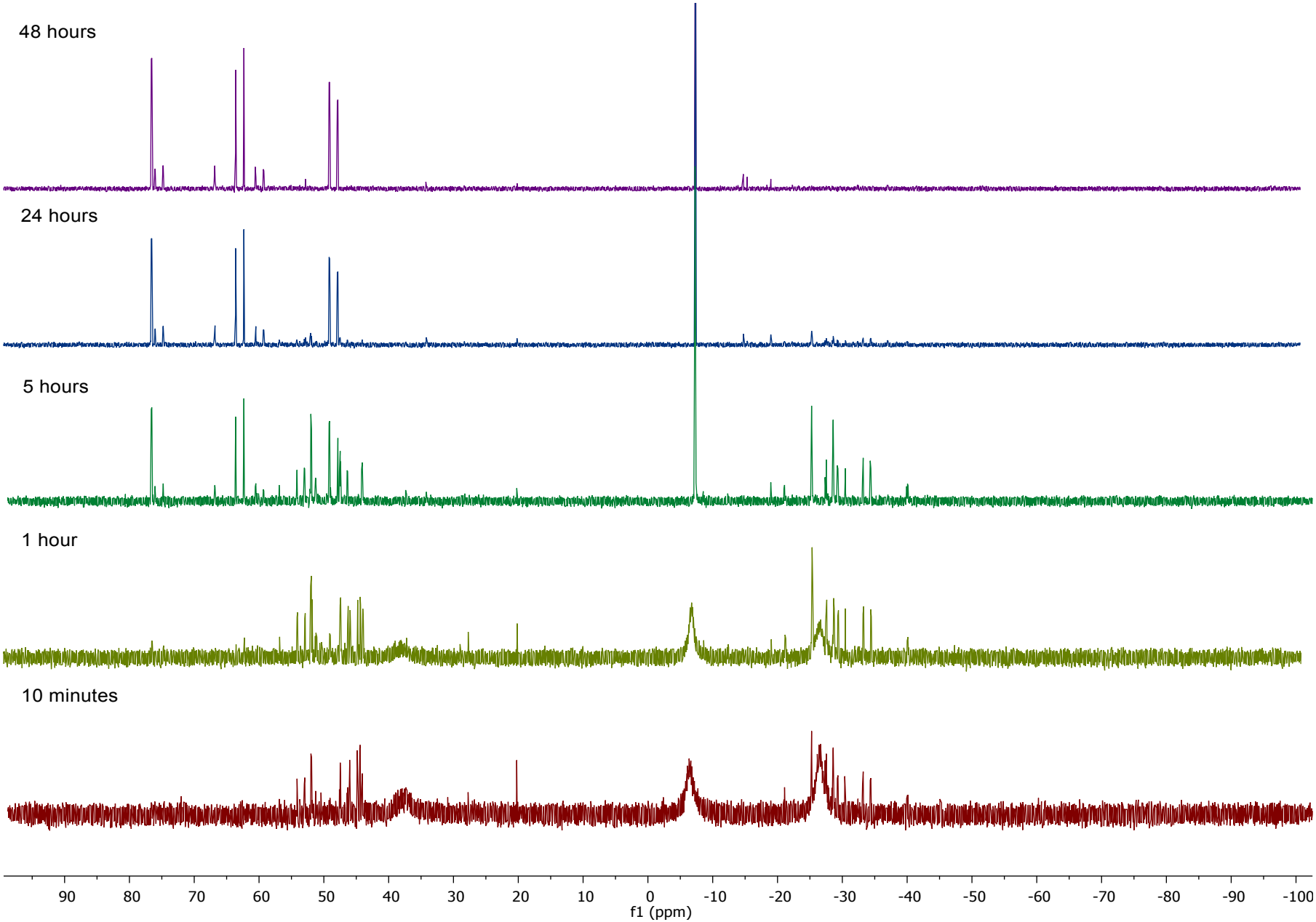


**Fig. S10.** $^{31}P\{^{1}H\}$ NMR spectra (202 MHz, THF-$d_8$, 298 K) demonstrating the progress of the reaction between $[Ru(PPh_3)_3Cl_2]\cdot PPh_3$ and $ZnMe_2$ at 298 K.

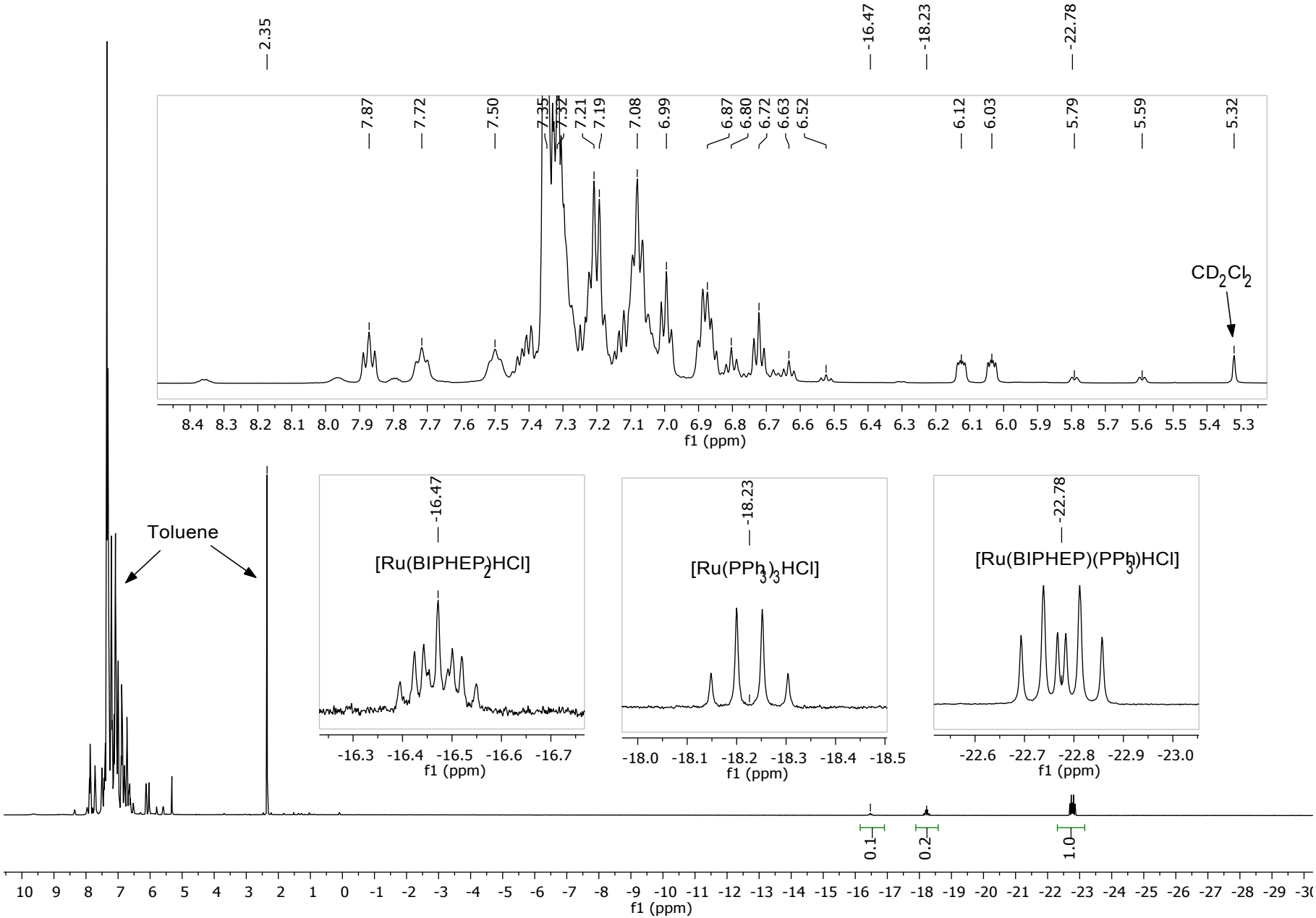


**Fig. S11.** $^{1}H$ NMR spectrum (500 MHz, $CD_2Cl_2$, 298 K) of [Ru(BIPHEP)($PPh_3$)HCl] formed *in-situ* from reaction of [Ru($PPh_3$)$_3$HCl] and BIPHEP.

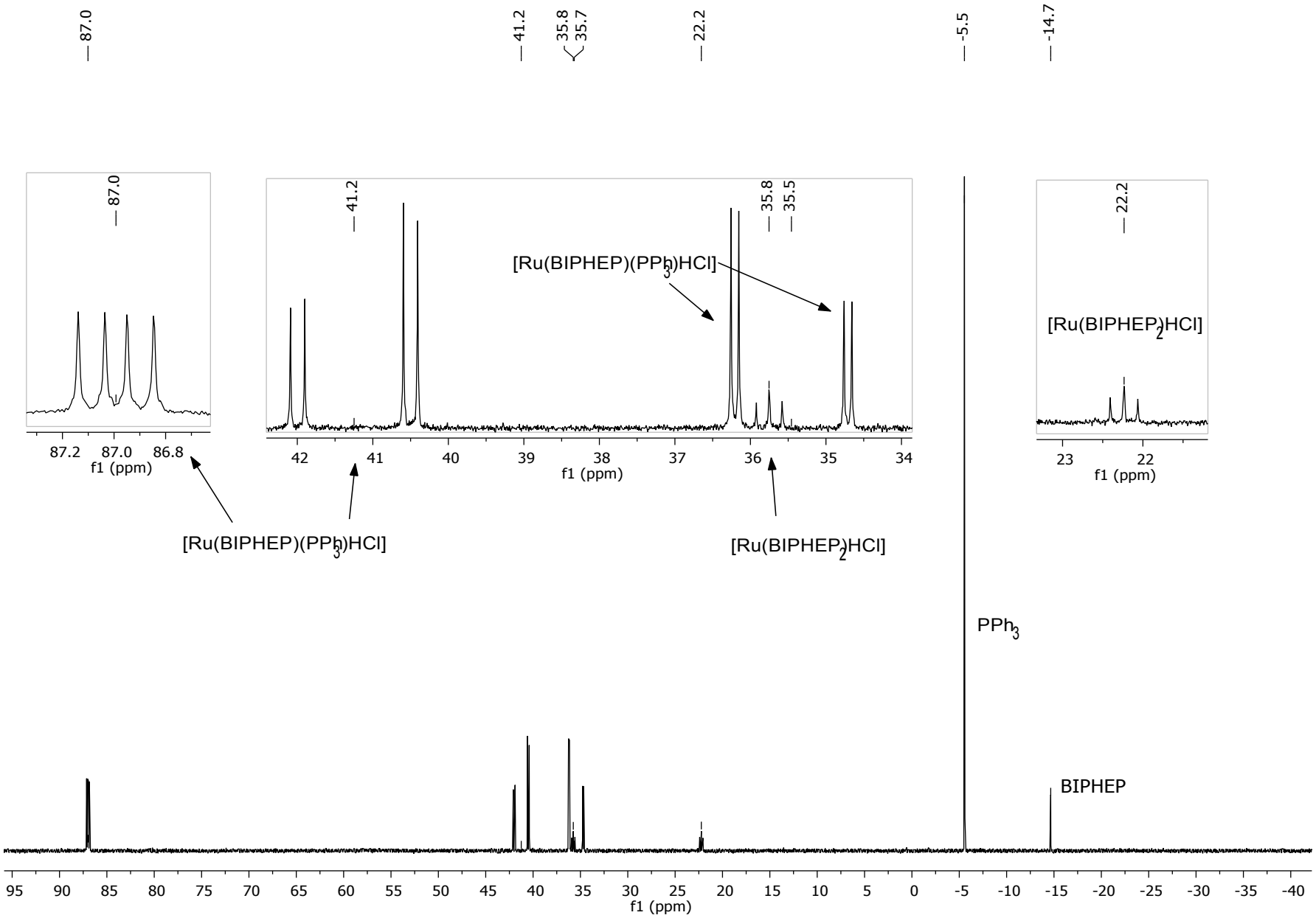


**Fig. S12.** $^{31}P\{^{1}H\}$ NMR spectrum (202 MHz, $CD_2Cl_2$) of [Ru(BIPHEP)($PPh_3$)HCl] formed *in-situ* in the reaction of [Ru($PPh_3$)$_3$HCl] and BIPHEP.

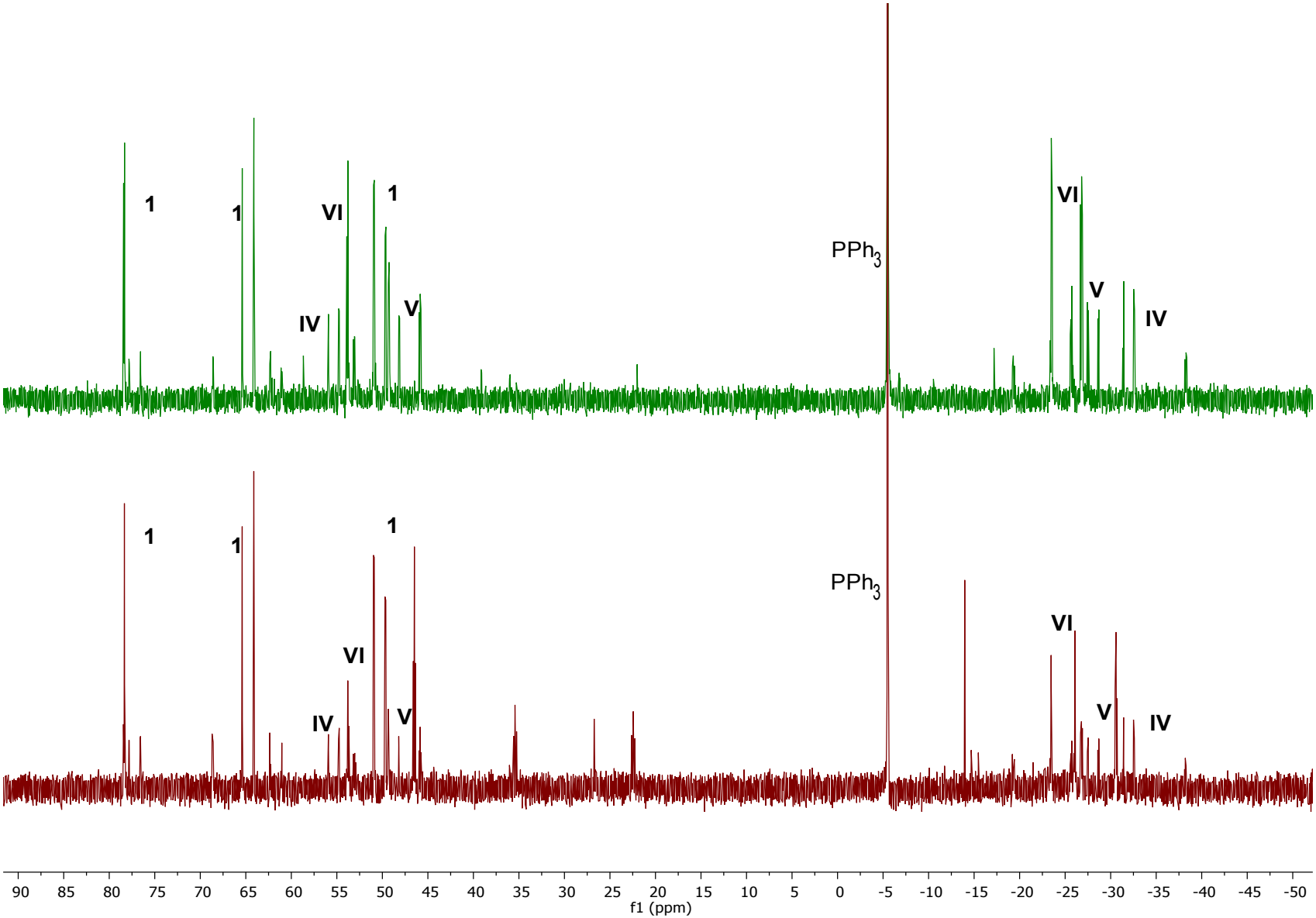


**Fig. S13.** Overlaid $^{31}P\{^{1}H\}$ NMR spectra (202 MHz, THF-$d_8$, 298 K) showing the reaction of $[Ru(PPh_3)_3Cl_2]\cdot PPh_3$ and $ZnMe_2$ after 5 h (top), and reaction of [Ru(BIPHEP)($PPh_3$)HCl] and $ZnMe_2$ (bottom). The spectra highlight the formation of late intermediates **IV**-**VI** and final product **1** in both reactions.

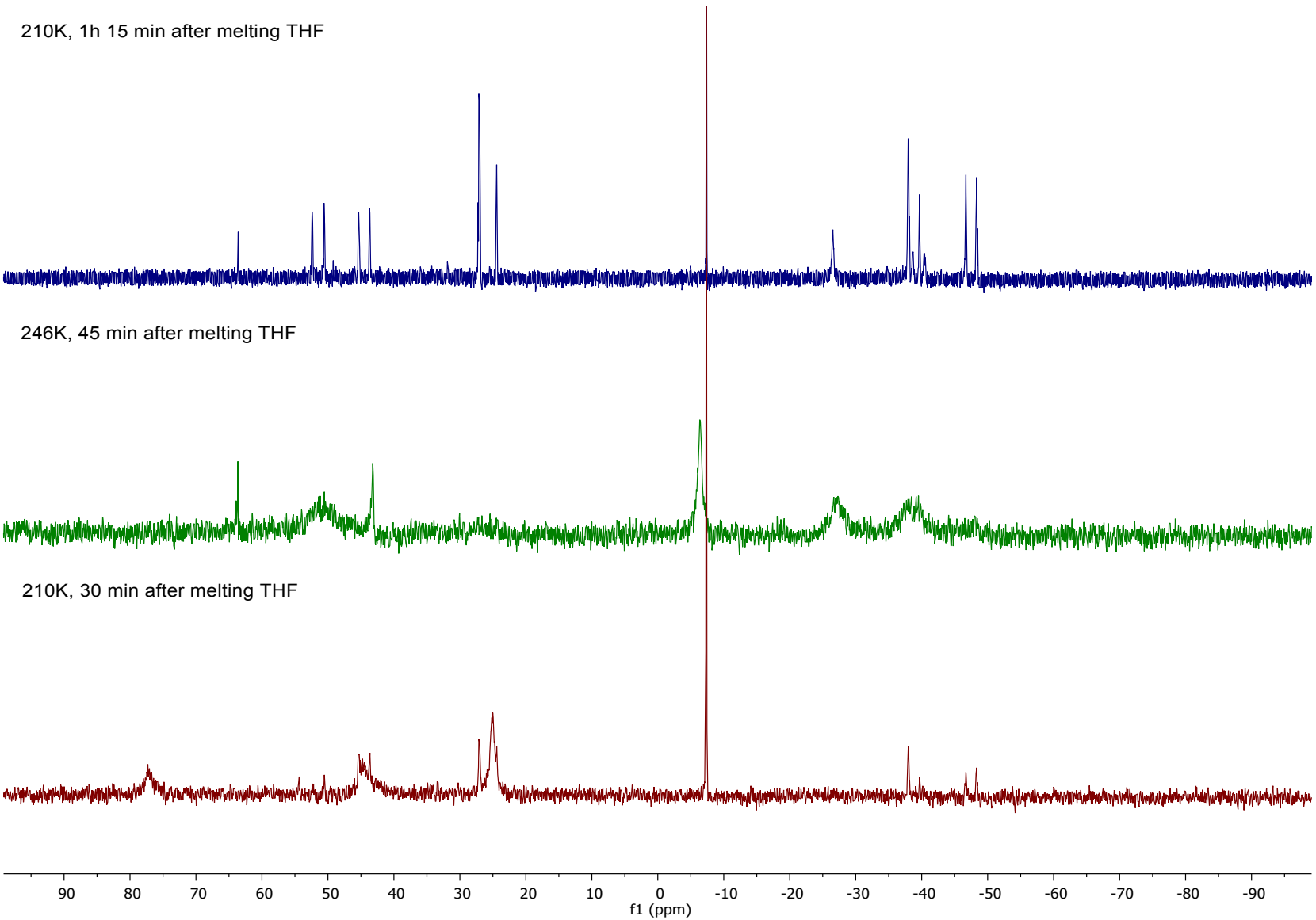


**Fig. S14.** VT $^{31}P\{^{1}H\}$ NMR spectra (162 MHz, THF-$d_8$) of the reaction of $[Ru(PPh_3)_3Cl_2]\cdot PPh_3$ and $ZnMe_2$, demonstrating the formation of early intermediates (**I-III**).

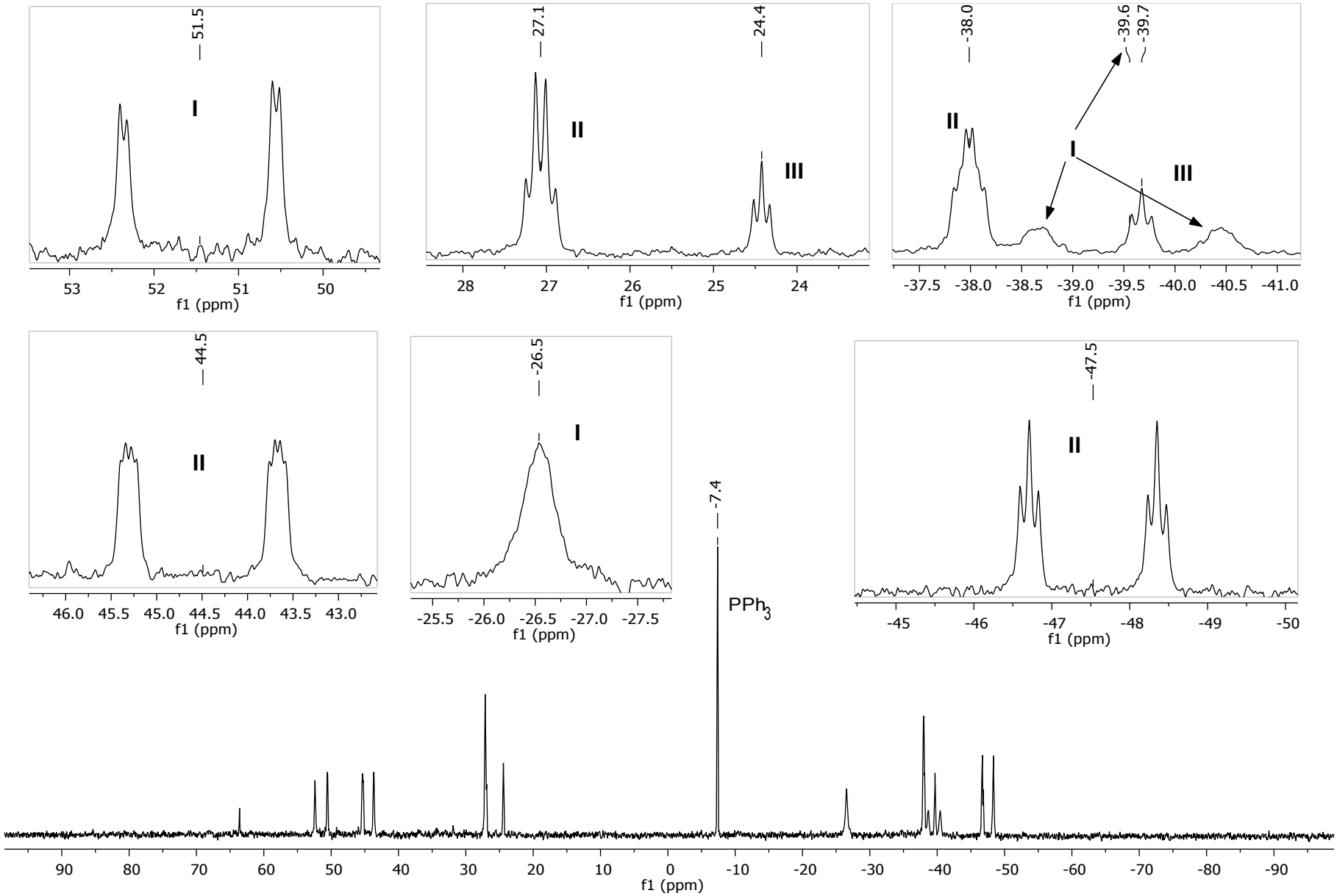


**Fig. S15.** $^{31}P\{^{1}H\}$ NMR spectrum (162 MHz, THF-$d_8$, 210 K) of reaction of $[Ru(PPh_3)_3Cl_2]\cdot PPh_3$ and $ZnMe_2$ at 246 K showing early intermediates **I-III**.

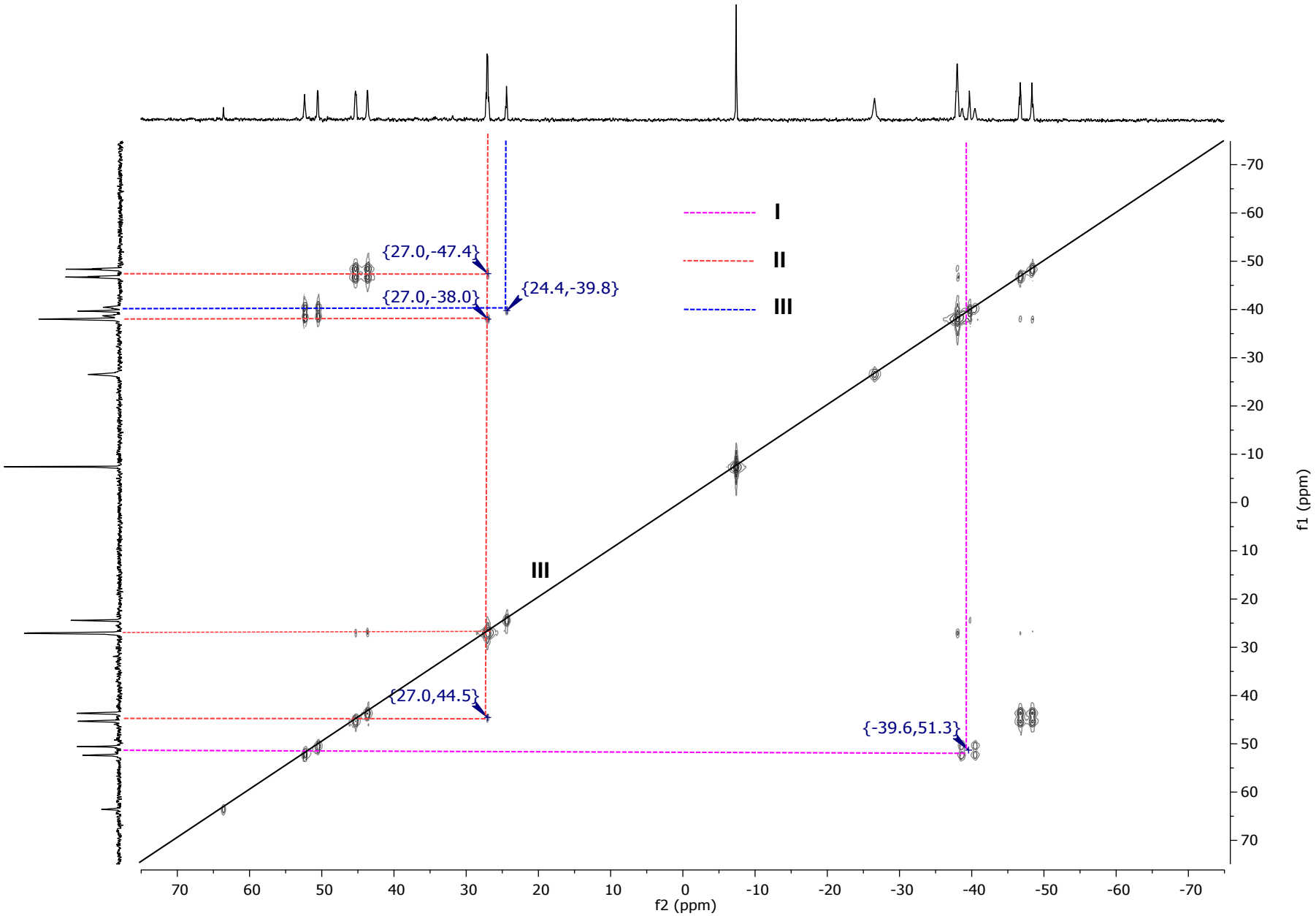


**Fig. S16.** $^{31}P\{^{1}H\}$ COSY (162 MHz, THF-$d_8$, 210 K) of reaction of $[Ru(PPh_3)_3Cl_2]\cdot PPh_3$ and $ZnMe_2$ at 246 K showing early intermediates **I-III**.

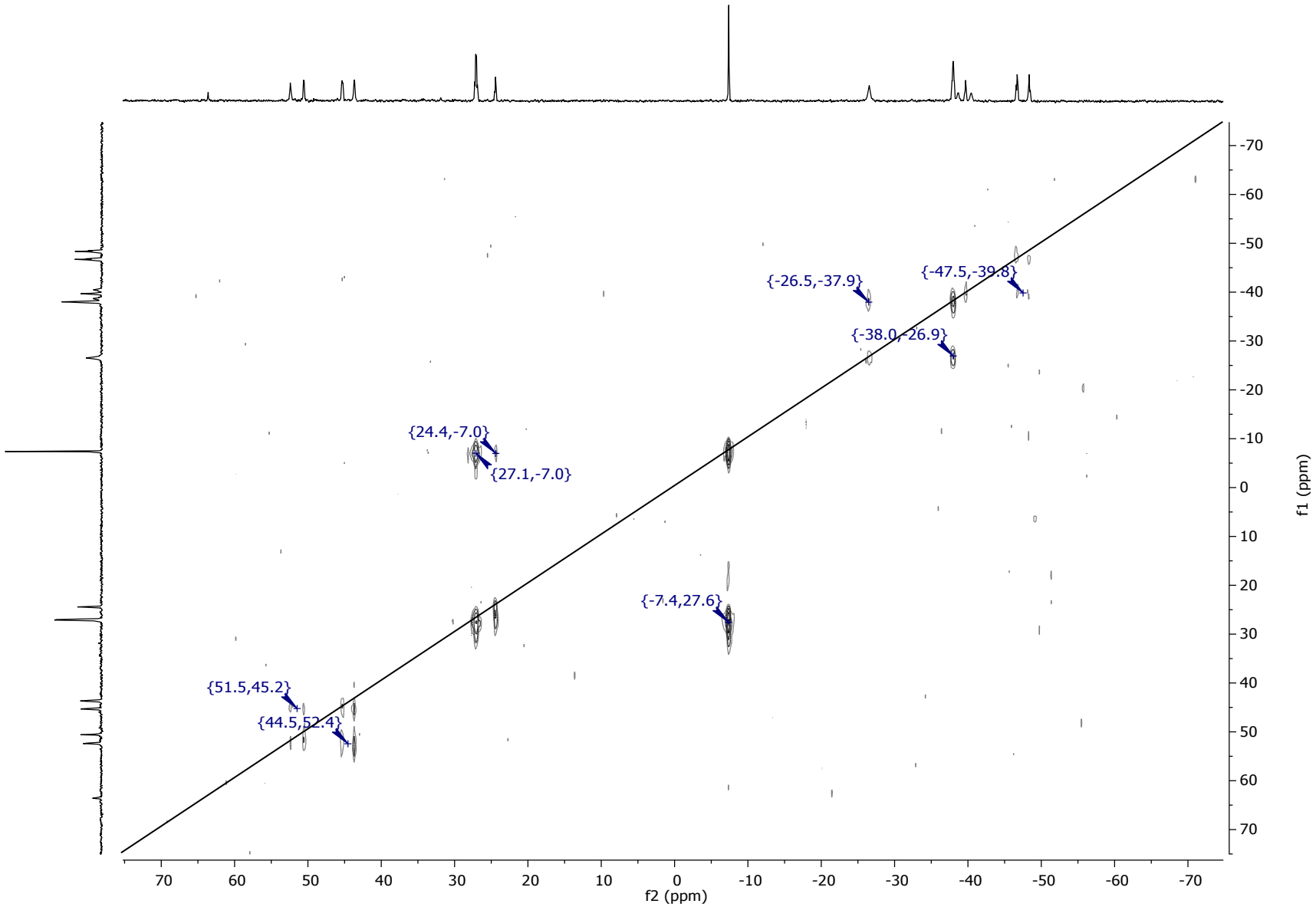


**Fig. S17.** $^{31}P\{^{1}H\}$ EXSY (162 MHz, THF-$d_8$, 210 K) of the reaction of $[Ru(PPh_3)_3Cl_2]\cdot PPh_3$ and $ZnMe_2$ at 246 K showing early intermediates **I-III**

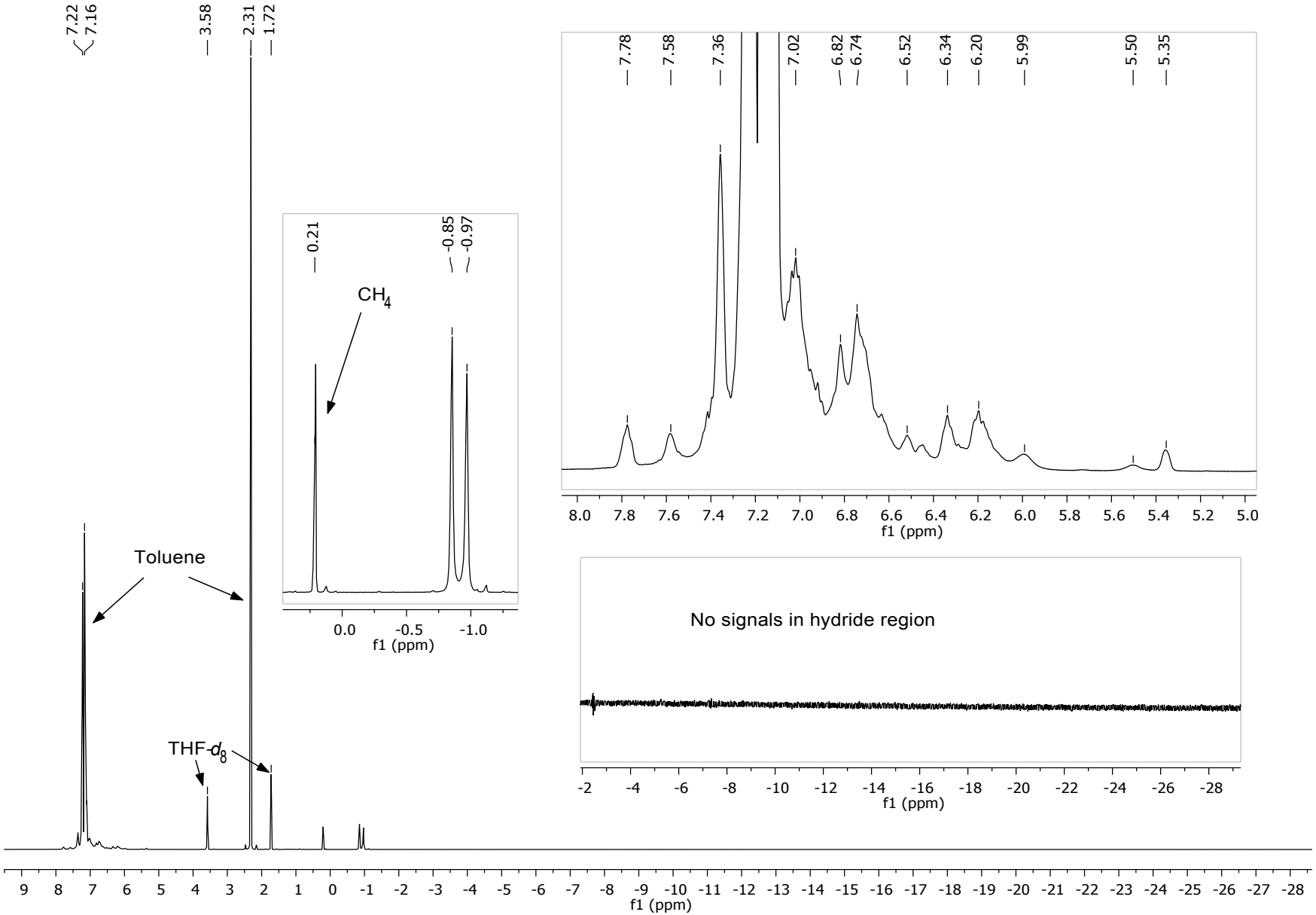


**Fig. S18.** $^1$H NMR spectrum (400 MHz, THF-$d_8$, 210 K) of the reaction of $[Ru(PPh_3)_3Cl_2]\cdot PPh_3$ and $ZnMe_2$ at 246 K showing early intermediates **I-III**.

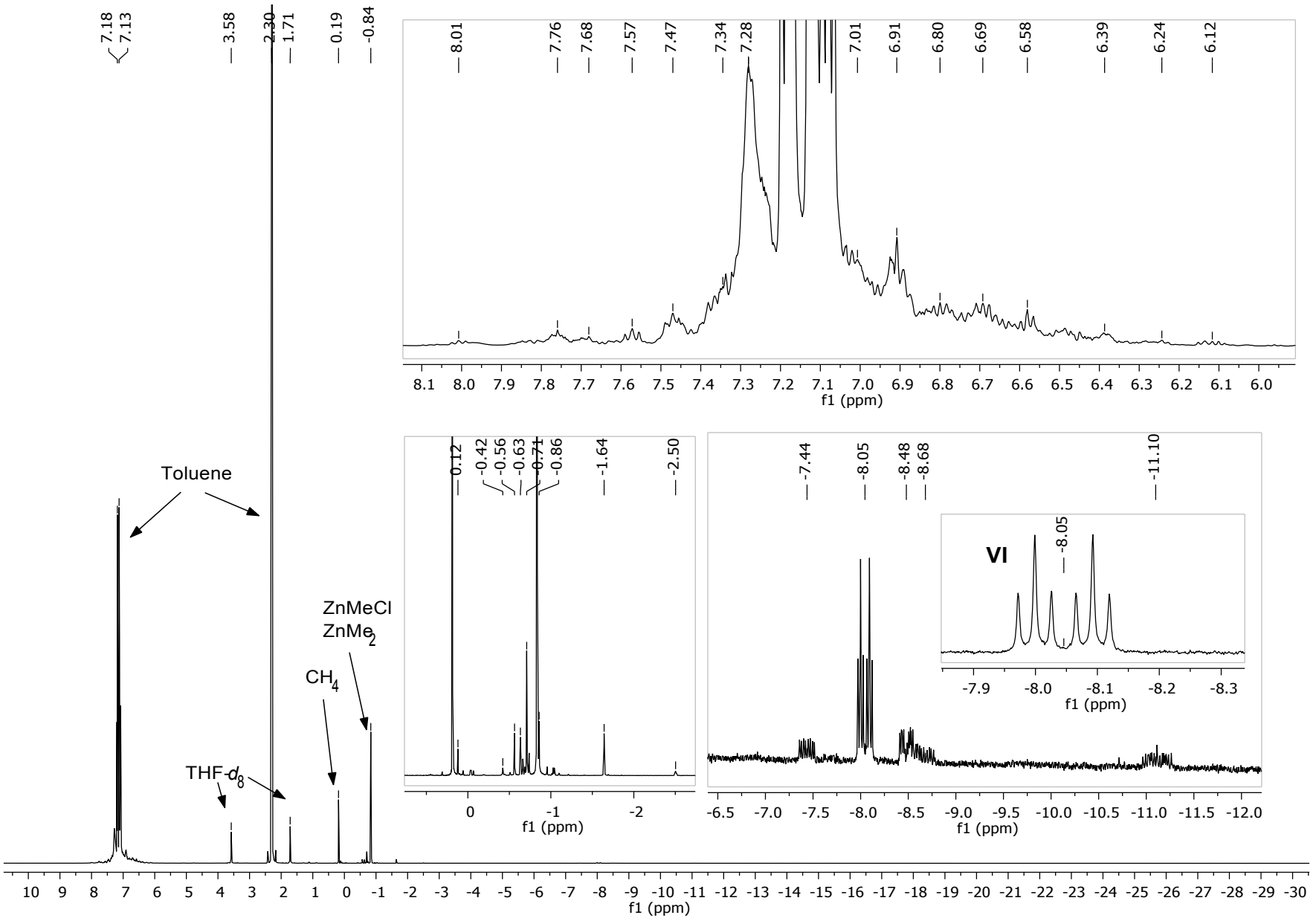


**Fig. S19.** $^{1}$H NMR spectrum (500 MHz, THF-$d_8$, 298 K) of the reaction of $[Ru(PPh_3)_3Cl_2]\cdot PPh_3$ and $ZnMe_2$ (3.5 h, 298 K) showing late intermediates **IV**-**VI**.

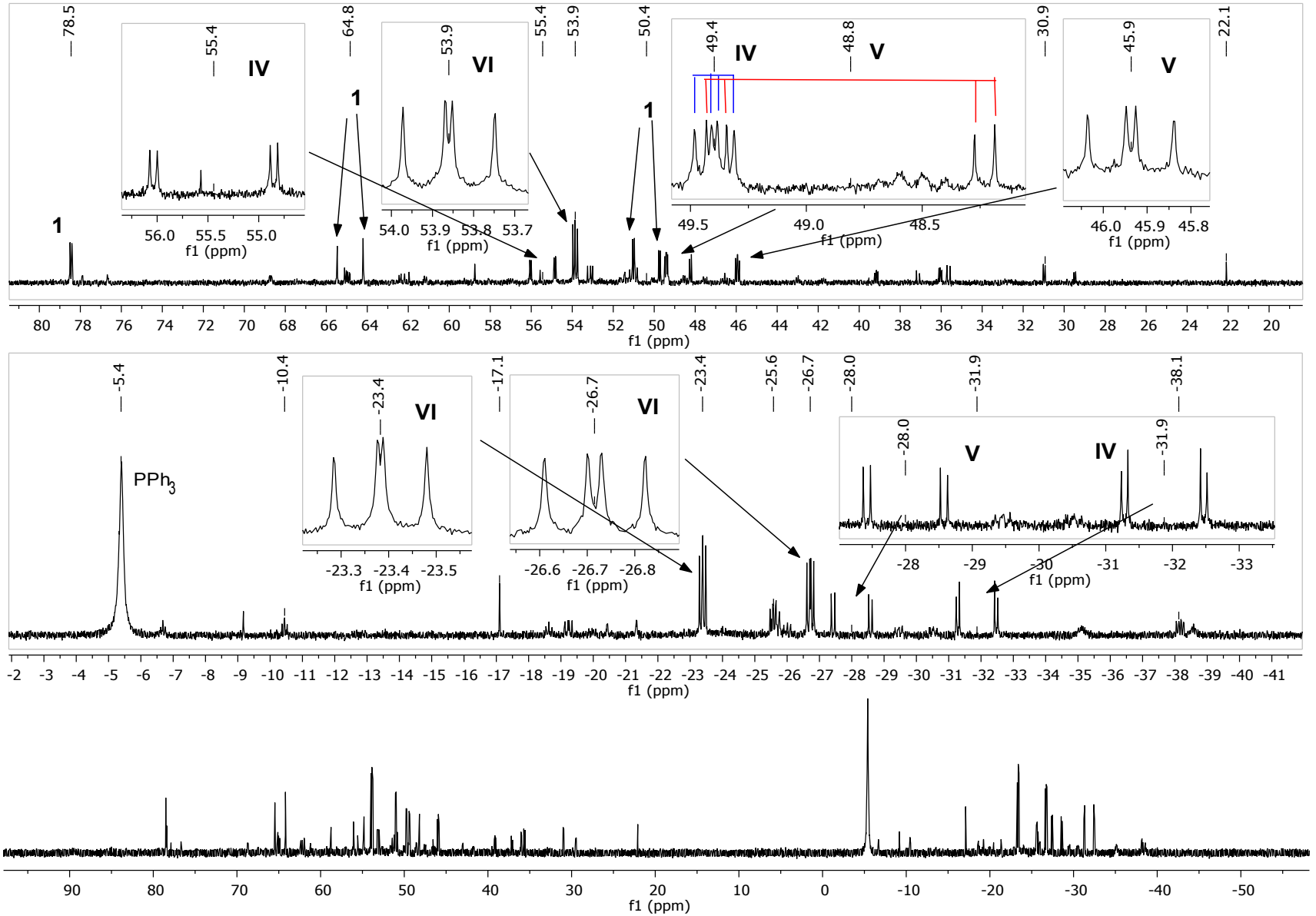


**Fig. S20.** $^{31}P\{^{1}H\}$ NMR spectrum (202 MHz, THF-$d_8$, 298 K) of the reaction of $[Ru(PPh_3)_3Cl_2]\cdot PPh_3$ and $ZnMe_2$ (4 h, 298 K) showing late intermediates **IV**-**VI**.

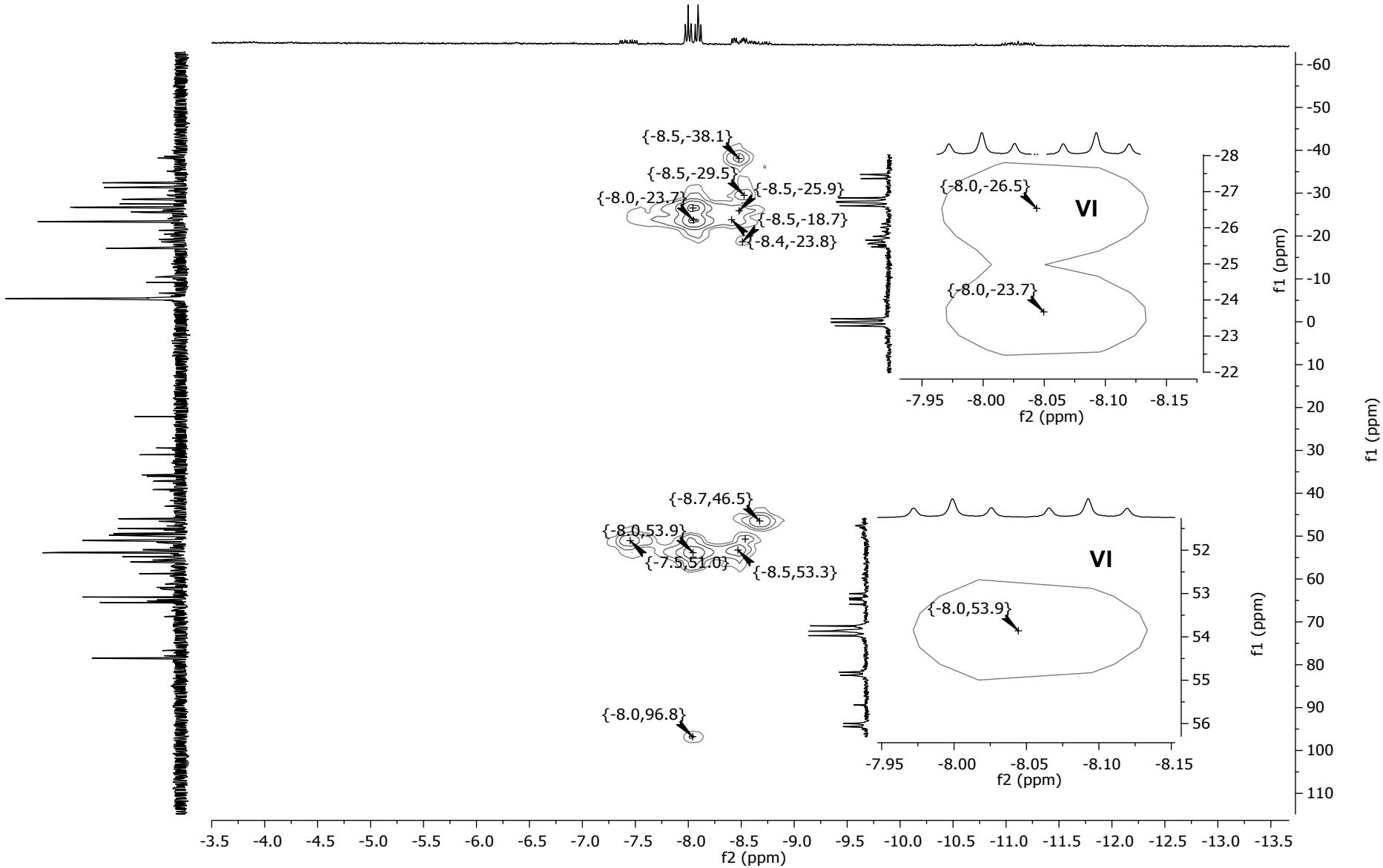


**Fig. S21.** $^{31}P\{^{1}H\}$ HMQC (202 MHz, THF-$d_8$, 298 K) of the reaction of $[Ru(PPh_3)_3Cl_2]\cdot PPh_3$ and $ZnMe_2$ after 5.5 h at 298 K showing late intermediates **IV**-**VI**.

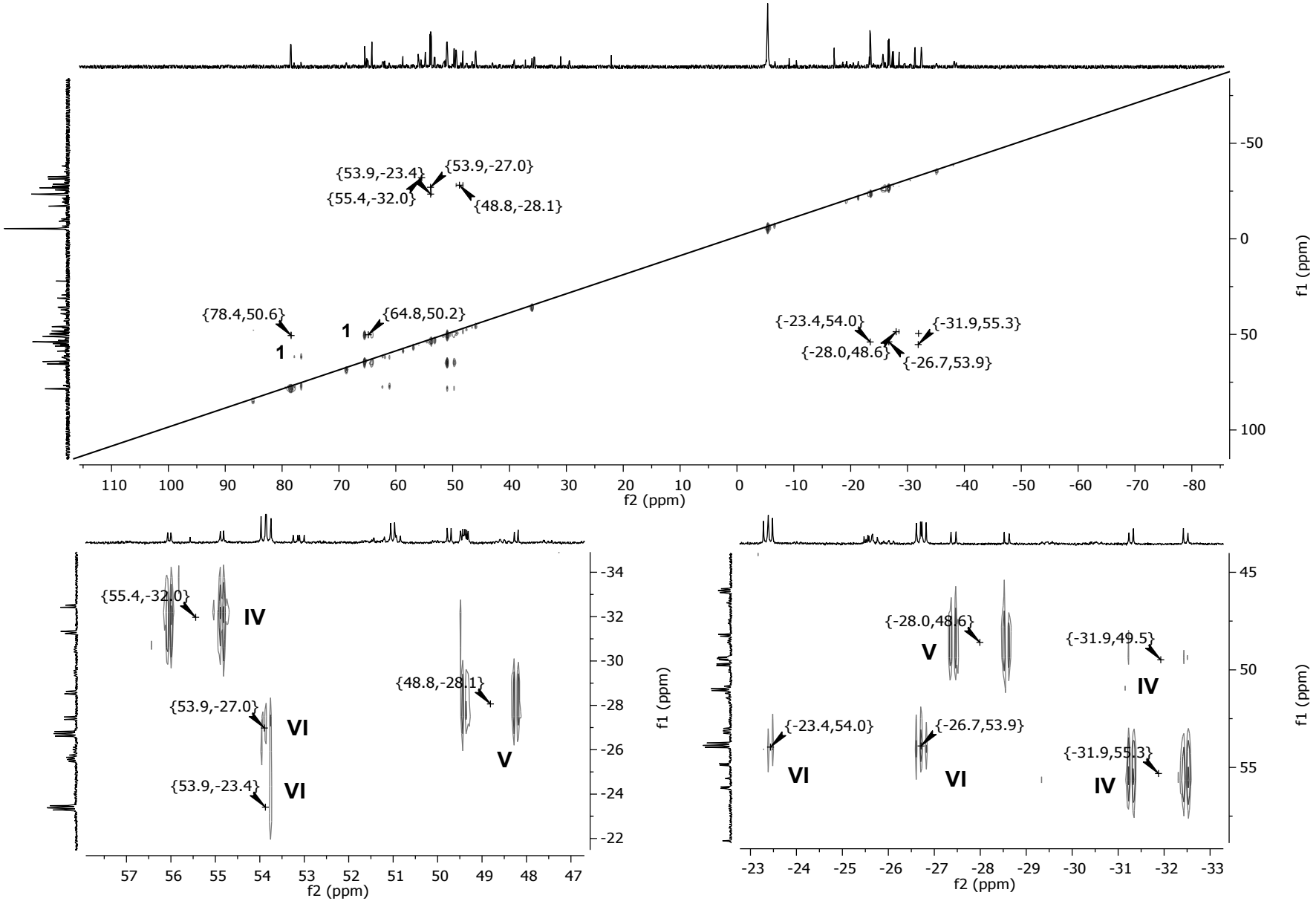


**Fig. S22.** $^{31}P\{^{1}H\}$ COSY (202 MHz, THF-$d_8$, 298 K) of reaction of $[Ru(PPh_3)_3Cl_2]\cdot PPh_3$ and $ZnMe_2$ after 7 h at 298 K showing late intermediates **IV**-**VI**.

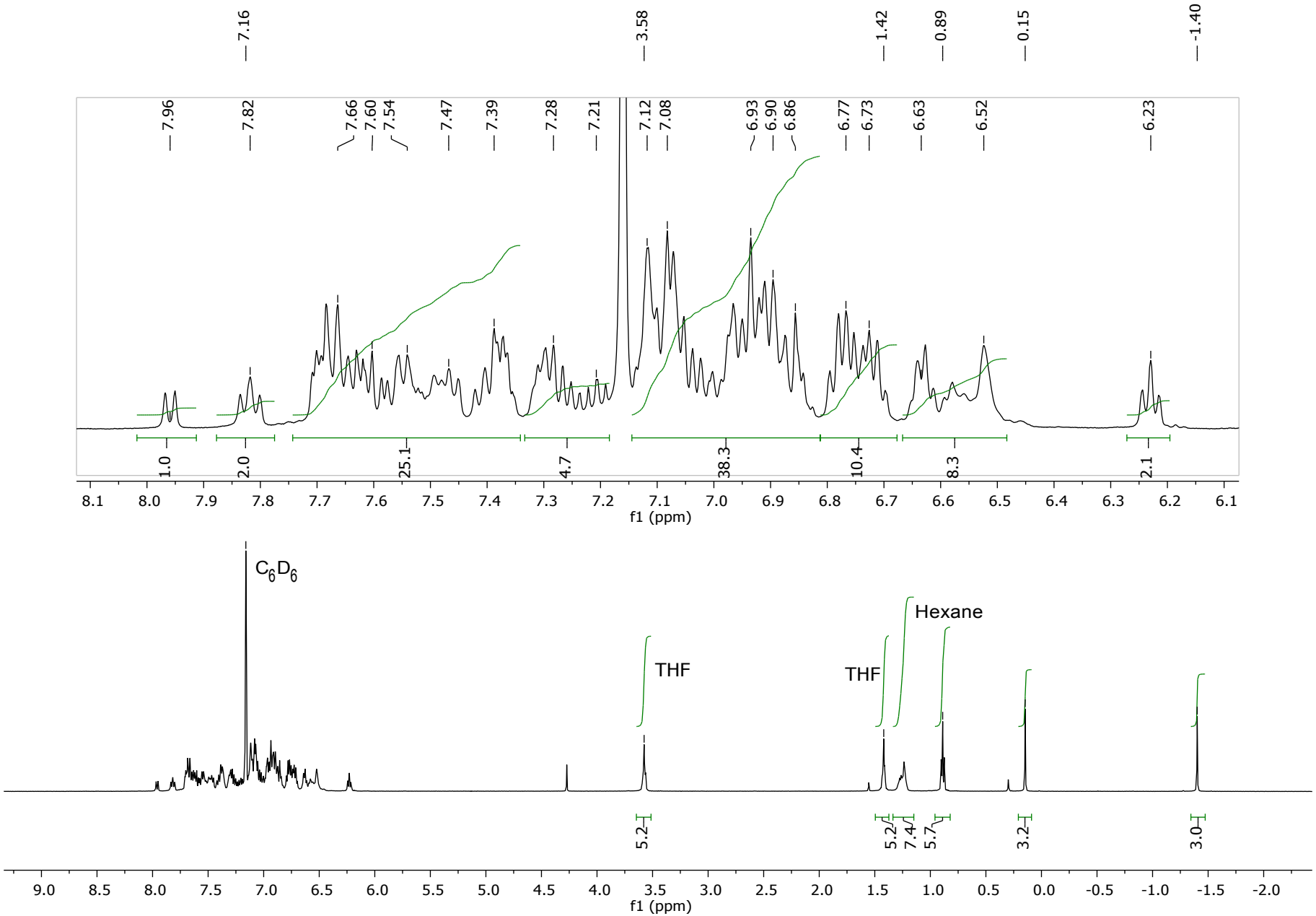


**Fig. S23.** $^{1}$H NMR spectrum (500 MHz, $C_6D_6$, 298 K) of [Ru(dppbz)($PPh_2$(binaphthyl)′)ZnMe] (**3**).

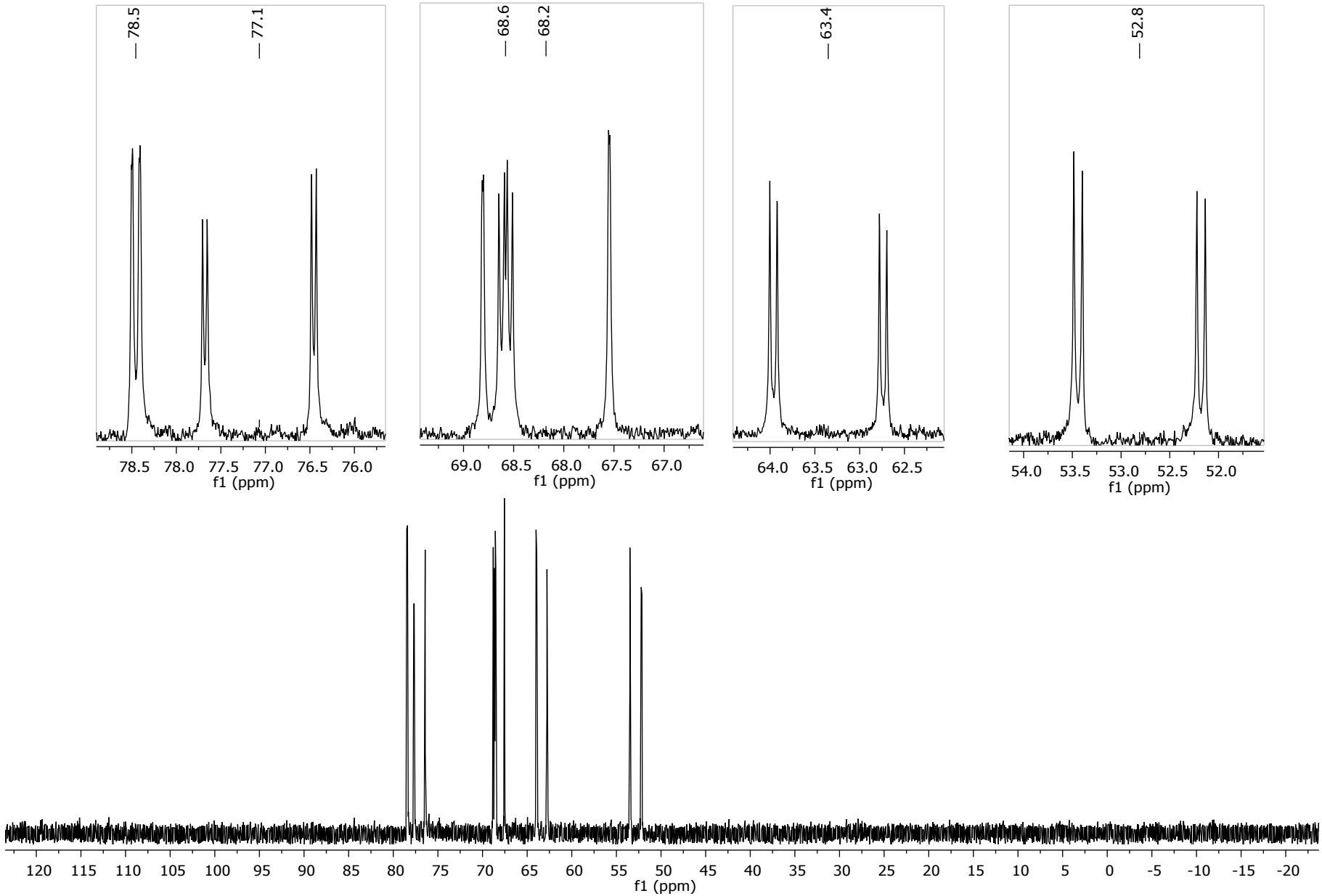


**Fig. S24.** $^{31}P\{^{1}H\}$ NMR spectrum (202 MHz, $C_6D_6$, 298 K) of [Ru(dppbz)($PPh_2$(binaphthyl)′)ZnMe] (**3**).

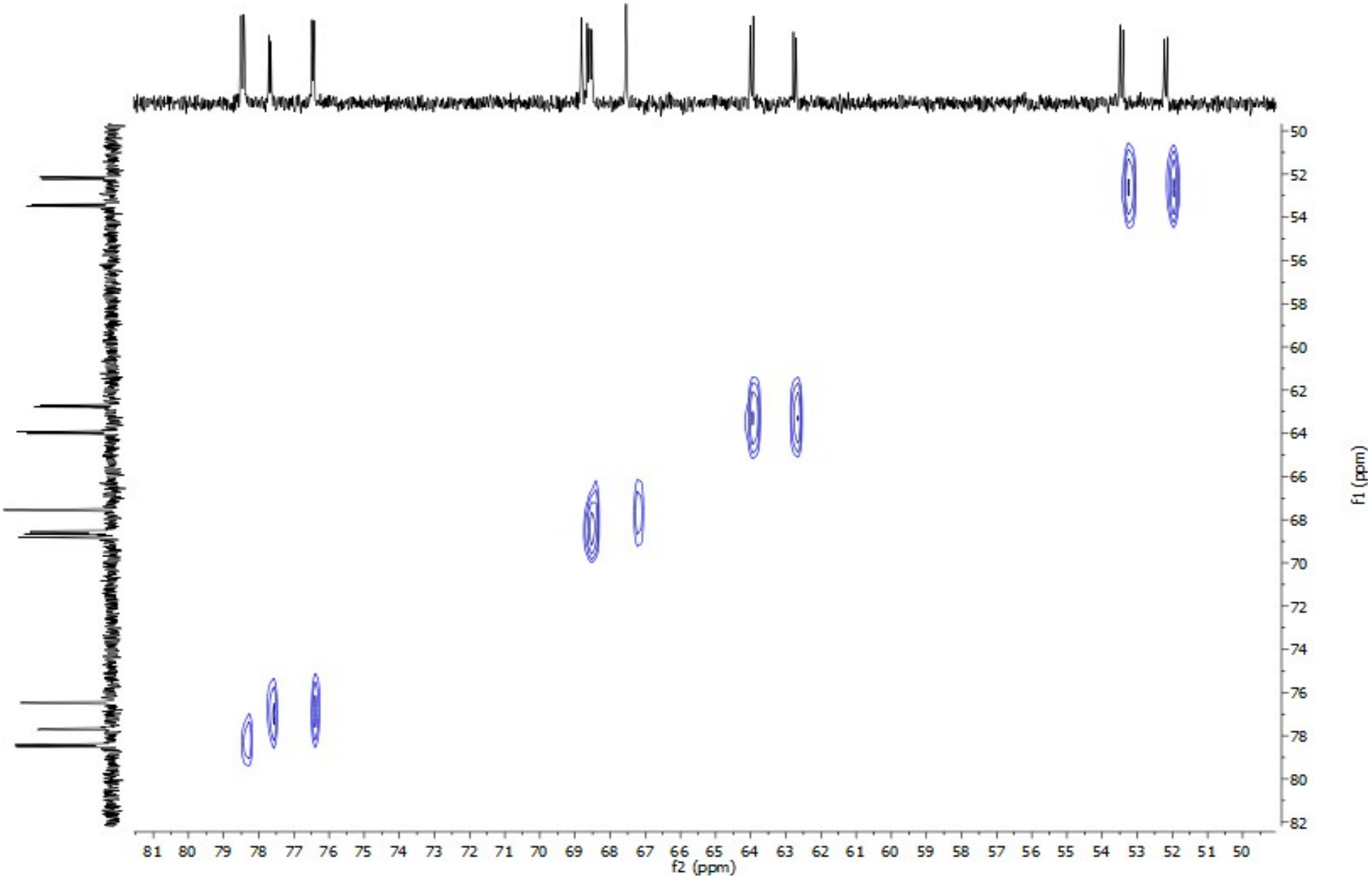


**Fig. S25.** $^{31}P\{^{1}H\}$ EXSY (202 MHz, $C_6D_6$, 298 K) of [Ru(dppbz)($PPh_2$(binaphthyl)′)ZnMe] (**3**), showing the lack of exchange of diastereomers.

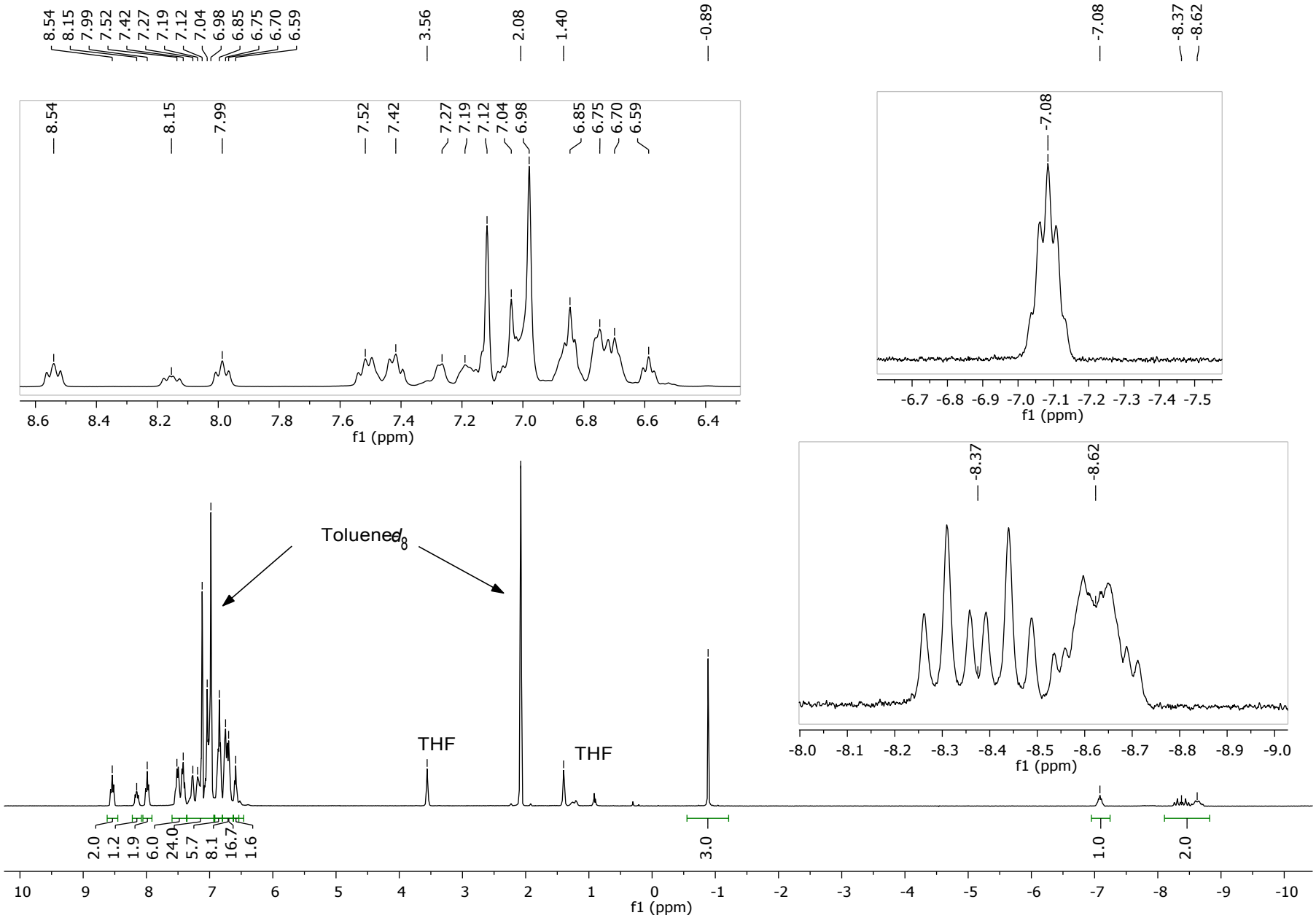


**Fig. S26.** $^{1}$H NMR spectrum (400 MHz, $C_6D_5CD_3$, 246 K) of the reaction of **1** and $H_2$ to give [Ru(dppbz)($Ph_2$P(biphenyl))$(H)_2$(H)(ZnMe)] (**4**).

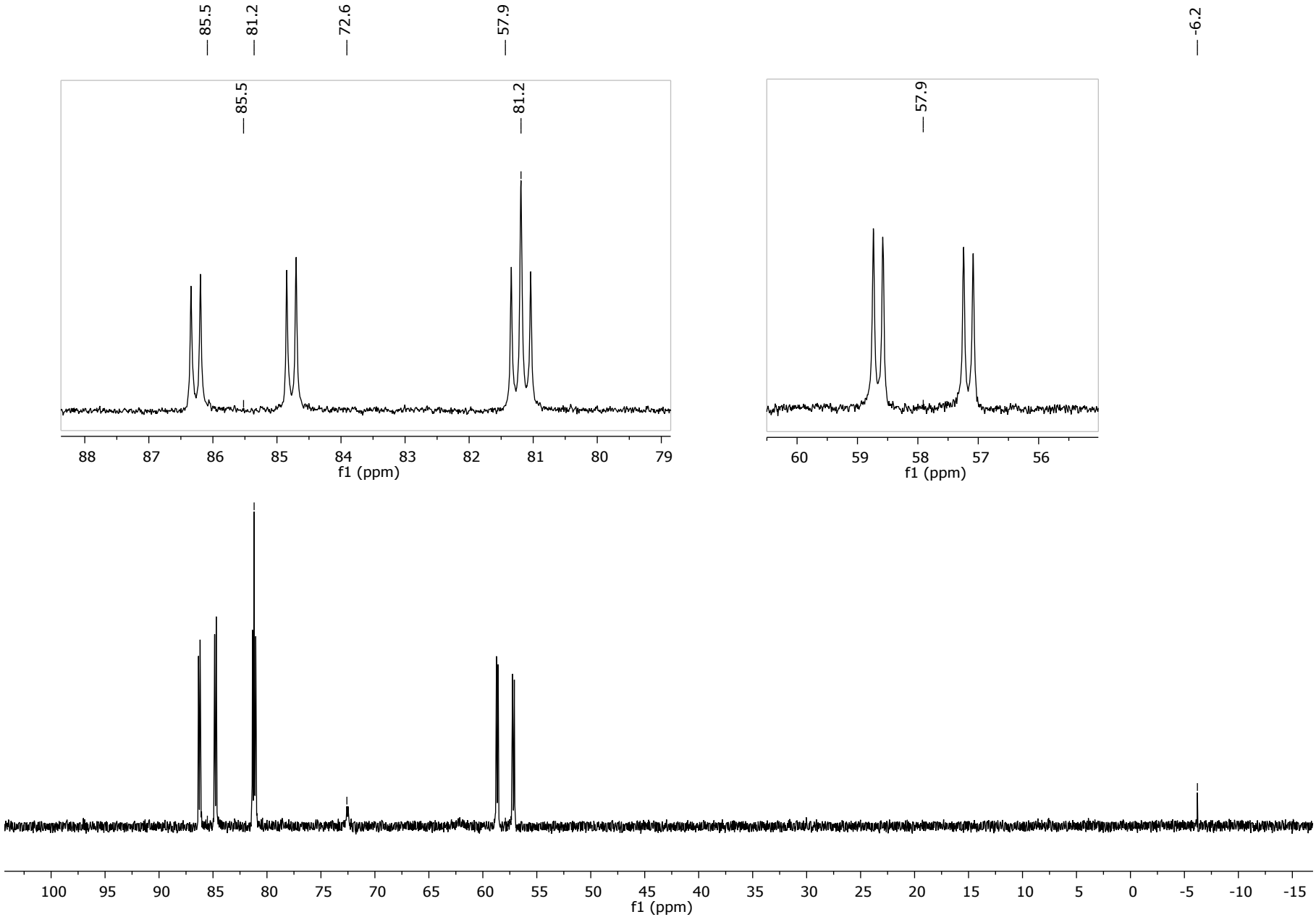


**Fig. S27.** $^{31}P\{^{1}H\}$ NMR spectrum (162 MHz, $C_6D_5CD_3$, 246 K) of reaction of **1** and $H_2$ to form [Ru(dppbz)($Ph_2P$(biphenyl))$(H)_2$(H)(ZnMe)] (**4**).

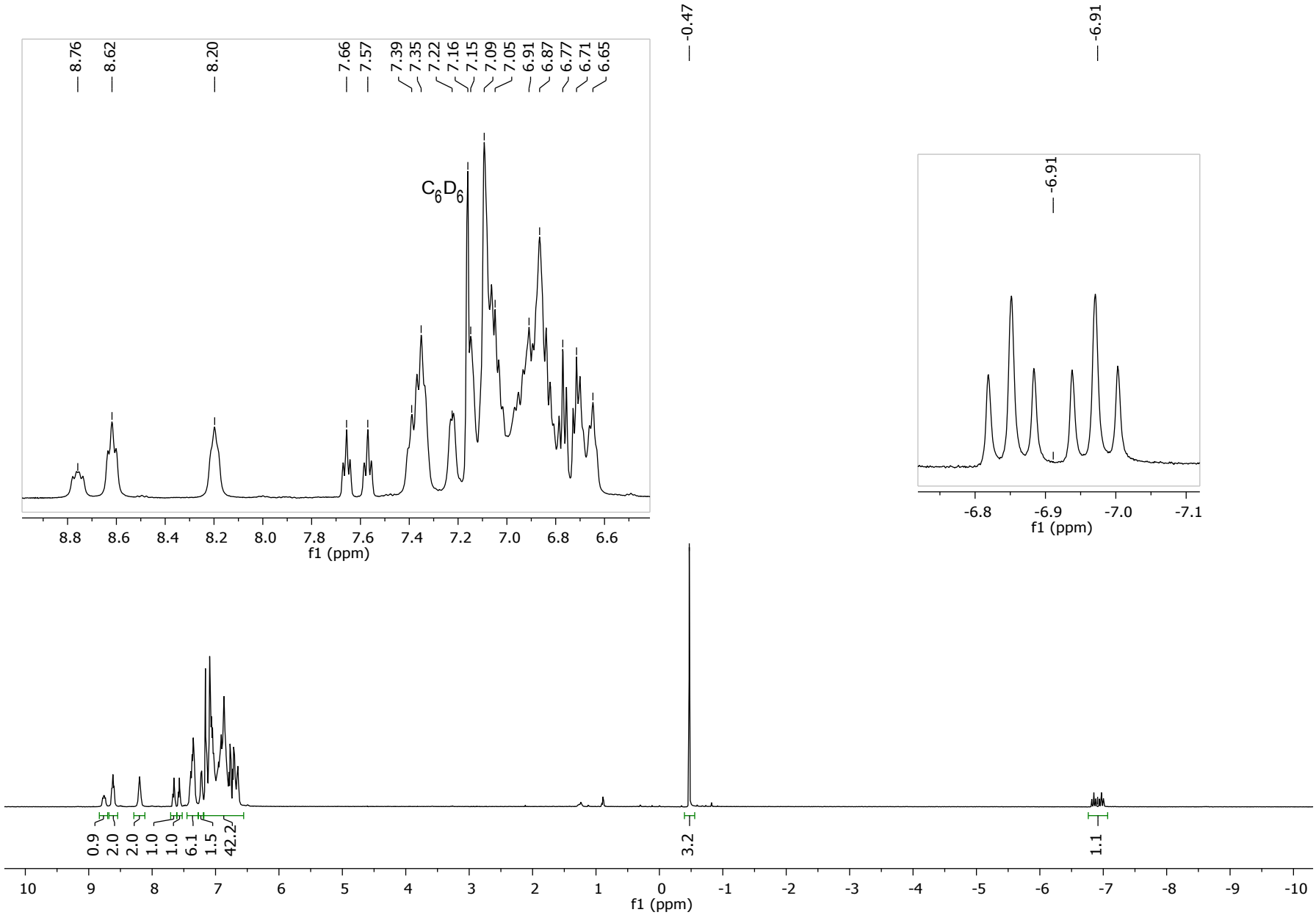


**Fig. S28.** $^{1}$H NMR spectrum (500 MHz, $C_6D_6$, 298 K) of [Ru(dppbz)($Ph_2$P(biphenyl))(C≡CPh)$_2$(H)(ZnMe)] (**5**).

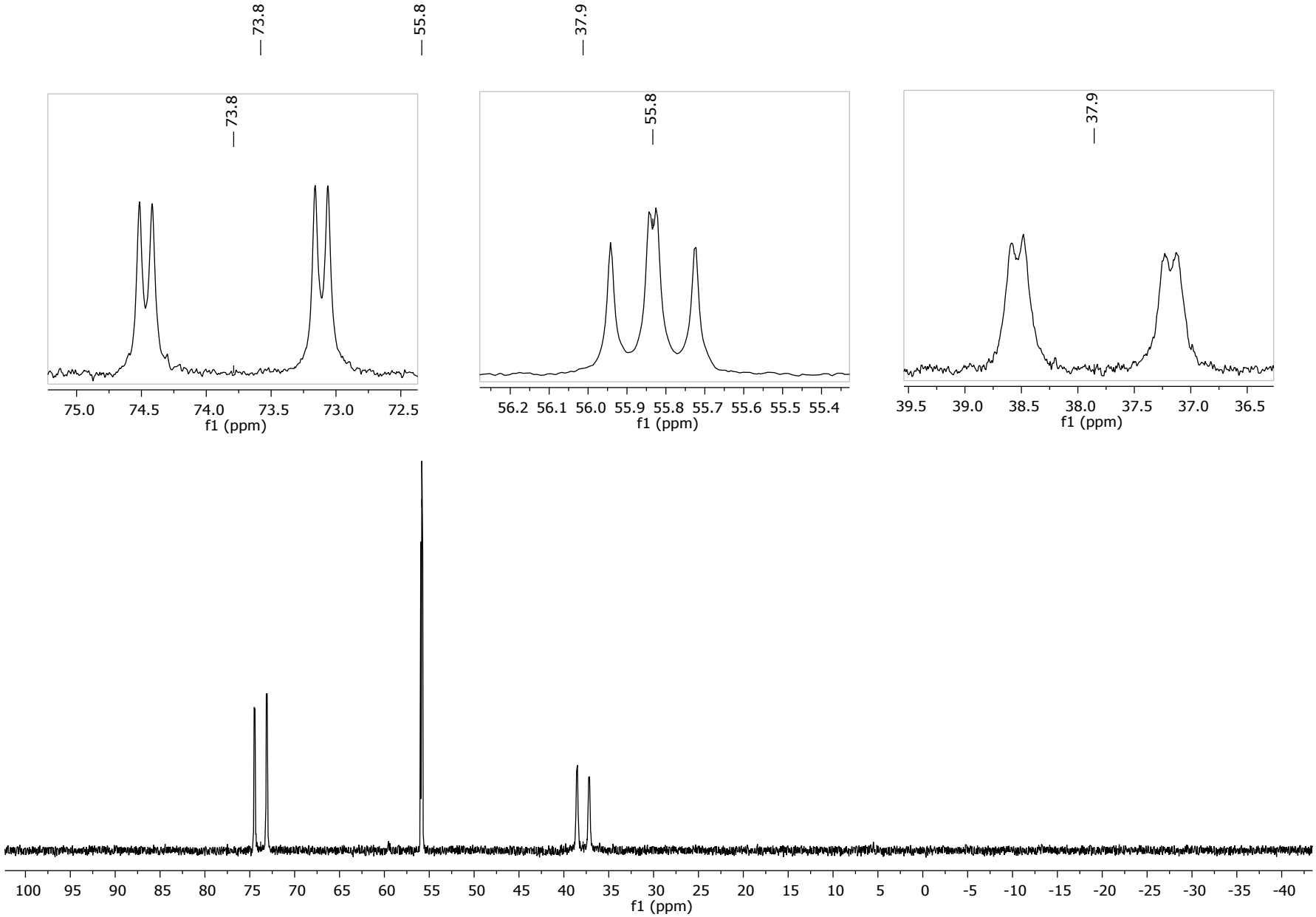


**Fig. S29.** $^{31}P\{^{1}H\}$ spectrum (202 MHz, $C_6D_6$, 298 K) of [Ru(dppbz)($Ph_2P$(biphenyl))($C{\equiv}CPh)_2$(H)(ZnMe)] (**5**).

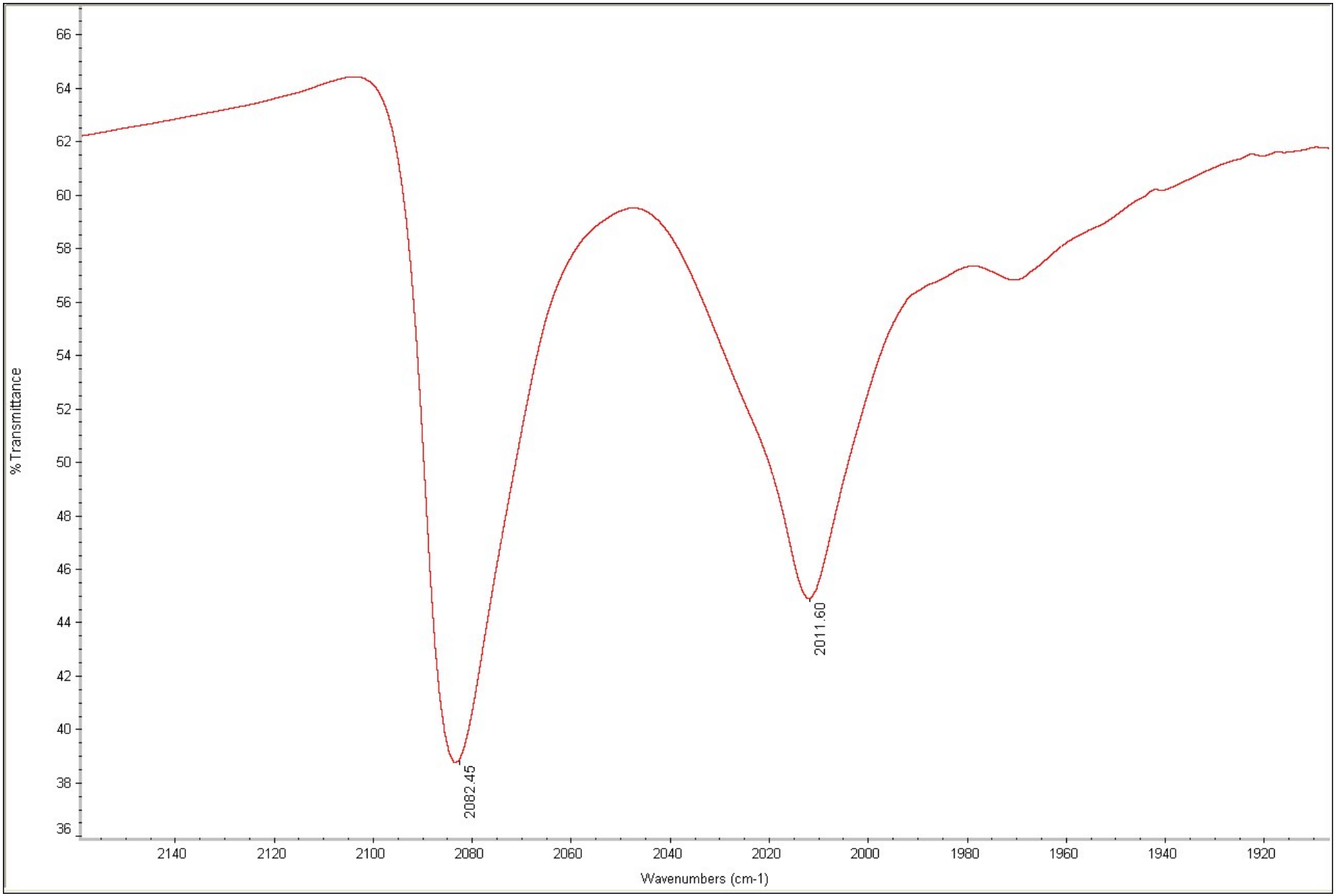


**Fig. S30.** IR spectrum (in KBr) showing ν(C≡C) of [Ru(dppbz)($Ph_2$P(biphenyl))(C≡CPh)$_2$(H)(ZnMe)] (**5**).

| Identification code | **1** | **3** | **5** |
|---|---|---|---|
| Empirical formula | $C_{56}H_{59}P_3RuZn$ | $C_{65}H_{53}P_3RuZnO_{0.5}$ | $C_{89}H_{75}P_3RuZn$ |
| Formula weight | 991.38 | 1101.42 | 1403.84 |
| Crystal system | monoclinic | triclinic | orthorhombic |
| Space group | $P2_1/c$ | $P$-1 | $Pbca$ |
| $a$/ Å | 11.0520(2) | 10.8687(2) | 17.33241(12) |
| $b$/ Å | 12.8732(2) | 12.1871(3) | 23.86672(17) |
| $c$/ Å | 36.3933(6) | 20.5157(5) | 33.9755(3) |
| $\alpha$/ ° | 90 | 79.451(2) | 90 |
| $\beta$/ ° | 98.665(2) | 81.396(2) | 90 |
| $\gamma$/ ° | 90 | 80.252(2) | 90 |
| $U$/ Å$^3$ | 5118.74(15) | 2613.17(11) | 14054.58(18) |
| $Z$ | 4 | 2 | 8 |
| $\rho_{calc}$/ g cm$^{-3}$ | 1.286 | 1.400 | 1.327 |
| $\mu$/ mm$^{-1}$ | 0.892 | 4.092 | 3.158 |
| $F$(000) | 2056.0 | 1132.0 | 5824.0 |
| Crystal size/ mm$^3$ | 0.577 × 0.42 × 0.383 | 0.169 × 0.136 × 0.064 | 0.124 × 0.108 × 0.069 |
| 2θ range for data collection/° | 6.724 to 52.792 | 8.03 to 146.214 | 6.818 to 146.212 |
| Index ranges | –9 ≤ h ≤ 13,<br>–16 ≤ k ≤ 15,<br>–45 ≤ l ≤ 45 | –13 ≤ h ≤ 8,<br>–15 ≤ k ≤ 15,<br>–25 ≤ l ≤ 25 | –19 ≤ h ≤ 21,<br>–27 ≤ k ≤ 29,<br>–39 ≤ l ≤ 42 |
| Reflections collected | 43780 | 30751 | 102521 |
| Independent reflections, $R_{int}$ | 10443, 0.0184 | 10334, 0.0333 | 14001, 0.0619 |
| Data/restraints/parameters | 10443/0/542 | 10334/265/858 | 14001/0/852 |
| Goodness–of–fit on F$^2$ | 1.119 | 1.028 | 1.014 |
| Final $R$1, $wR$2 [$I$>=2σ($I$)] | 0.0297, 0.0662 | 0.0306, 0.0734 | 0.0293, 0.0715 |
| Final $R$1, $wR$2 [all data] | 0.0321, 0.0671 | 0.0338, 0.0755 | 0.0346, 0.0749 |
| Largest diff. peak/hole/ e Å$^{-3}$ | 0.44/–0.44 | 0.67/–0.60 | 0.59/–0.71 |

**Table S1.** Crystal data and structure refinement details for **1**, **3** and **5**.